DNA Immobilization onto Electrochemically Functionalized Surfaces For Direct Detection of Hybridization

Arghavan Shabani

A Thesis

in

The Department

of

Chemistry and Biochemistry

Presented in Partial Fulfillment of the Requirements
for the Degree of Master of Science (Chemistry)
at Concordia University
Montreal, Quebec, Canada

March 2006

Your file Votre référence
ISBN: 0-494-14231-6
Our file Notre référence
ISBN: 0-494-14231-6

Abstract

DNA Immobilization onto Electrochemically Functionalized Surfaces For Direct Detection of Hybridization

Two different methods were used to modify surfaces for covalent attachment of single stranded DNA probe sequences. In the first protocol, n-type Si (100) surfaces were modified by reduction of 4-nitrobenzendiazonium through cyclic voltammetry.

Contact mode AFM was employed to produce holes in the deposited layer to determine layer thickness. Layer thickness was found to increase with the number of cyclic potential scans in both aqueous and acetonitrile media. In acetonitrile the layer thickness, after a single cyclic scan, was determined to be approximately 15 nm whereas, after three cyclic scans, the layer thickness was found to be approximately 35 nm. Layer thicknesses were also measured by ellipsometry and are in good agreement with the AFM results.

In the second protocol, screen-printed carbon electrodes were functionalized using 1-ethyl-3-(3-dimethylaminopropyl)-carbodiimide, under an applied potential of +2.2 V in aqueous acidic media. Both functionalized silicon and carbon surfaces were used to immobilize single stranded DNA-C_6NH_2 sequences. Probe oligonucleotides were then attached to these surfaces and their hybridization with complementary strands was confirmed by fluorescence measurements. Electrochemical impedance measurements were used to detect hybridization of immobilized DNA. A significant shift in the flat band potential confirmed the hybridization event.

Acknowledgment

I would like to express my great appreciation to my research supervisors, Prof. Marcus Lawrence and Prof. Louis Cuccia for their excellent coaching, the best guidance and strong support through this project. Their help and encouragement facilitated the work in this thesis.

I wish to thank my research committee Dr. Christine E. DeWolf and Dr.Yves Gélinas for their comments and their review of this thesis. I would also to thank Dr. Rolf. Schmidt for his assistance in ellipsometery and AFM instrumentation.

Finally, I would like to express my heartfelt thanks to my family and friends, especially my mother, without their support and encouragement this work would not have been possible.

Table of Contents

List of Figures

List of Tables

List of Schemes

List of Abbreviations

DNA	Deoxyribonucleic acid
EDC	1-Ethyl-3-(3-dimethylaminopropyl)-carbodiimide
SPEs	Screen-printed electrodes
RNA	Ribonucleic acid
C	Cytosine
G	Guanine
A	Adenine
T	Thymine
U	Uracil
V_B	Valence band
C_B	Conduction band
E_g	Band gap energy
E_f	Fermi level
V_{fb}	Flat band potential
Z	Impedance
ac	Alternating current
dc	Direct current
V	Potential
I	Current
Z_r	Real impedance
Z_i	Imaginary impedance
EIS	Electrolyte/Insulator/ Semiconductor

SPM	Scanninig probe microscopy
AFM	Atomic Force Microscope
SFM	Scanning Force Microscope
XPS	X-ray photoelectron spectroscopy
ESCA	Electron spectroscopy for chemical analysis
TBAHFP	Tetrabutyl ammonium hexafluorophosphate
PMT	Photomultiplier tube

I. Introduction

In the field of biotechnology there has been considerable attention focused on surface functionalization for the immobilization of biomolecules onto transducers. The realization of such surfaces for use in biosensors to detect nucleic acids, for analysis of genetic disorders or genome sequencing, is of current major interest [1-4].

The approaches used to immobilize DNA probes onto solid supports represent a crucial step in the development of DNA biosensors capable of efficient hybridization detection and good reproducibility. Different strategies have been used to immobilize oligonucleotides onto surfaces, which include: thiolated DNA for self-assembly onto gold transducers [5,6], covalent immobilization of oligonucleotides on screen printed carbon electrodes (SPEs) [7], simple adsorption of nucleic acids on carbon surfaces [8] and mica [9], covalent coupling reaction of oligonucleotides with APTS (aminopropyl triethoxysilane) [10] and GPTS (3-glycidoxy propyltrimethoxysilane) on Si/SiO_2 chips[11,12], and covalent immobilization of thiol-terminated DNA on self-assembled layers of MPTS (3-mercaptopropyltrimethoxysilane) *via* disulfide linkages [13].

Covalent attachment of oligonucleotides to a chemically functionalized surface is advantageous because it not only allows for more rigorous washing to reduce non-specific adsorption, but it also prevents the loss of probe oligonucleotides from the surface. The electrochemical reduction of diazonium derivatives is one important route for surface functionalization, which was first reported in 1992 by Delamar *et al.*[14]. The mechanism of attachment can be explained by the generation of aryl radicals and subsequent formation of covalent bonds between the surface and the aryl groups [15].

The electrochemical reduction of diazonium salts has been studied with a variety of techniques including electrochemistry [16], X-ray photoelectron spectroscopy (XPS) [17], IR spectroscopy [18] , Rutherford backscattering spectroscopy[15], scanning probe microscopy (SPM) [19] and involves different substrates such as glassy carbon (GC) [20], highly oriented pyrolytic graphite (HOPG) [21], screen-printed carbon electrodes (SPEs) [22], pyrolyzed photoresist films (PPFs) [23], Pt [24], ultrananocrystalline diamond [25] and Si [26]. Among these materials, Si is an attractive substrate because it is available as a high purity, microelectronic grade material, with well-known surface properties. Well-ordered, hydrogen terminated, atomically flat silicon surfaces can be prepared and easily modified through electrochemical reduction of diazonium compounds.

In this work two different methods have been chosen for the covalent attachment of oligonucleotides to electrochemically functionalized surfaces. In the first method, silicon (100) surfaces were functionalized by a simple 2-step cyclic voltammetric reduction process using a diazonium salt as starting compound, and then treated with glutaraldehyde to act as a linker for the attachment of the oligonucleotide (see idealized representation, Scheme 1.1). In the second protocol, binding of oligonucleotides to screen-printed carbon electrodes (SPEs) was achieved through electrochemical modification of the surface with 1-ethyl-3-(3-dimethylaminopropyl)-carbodiimide (EDC).

The functionalized surfaces were analyzed using atomic force microscopy, ellipsometry and X-ray photoelectron spectroscopy. Probe oligonucleotides were then attached to these surfaces and their hybridization with complementary strands was confirmed by fluorescence measurements and impedance spectroscopy.

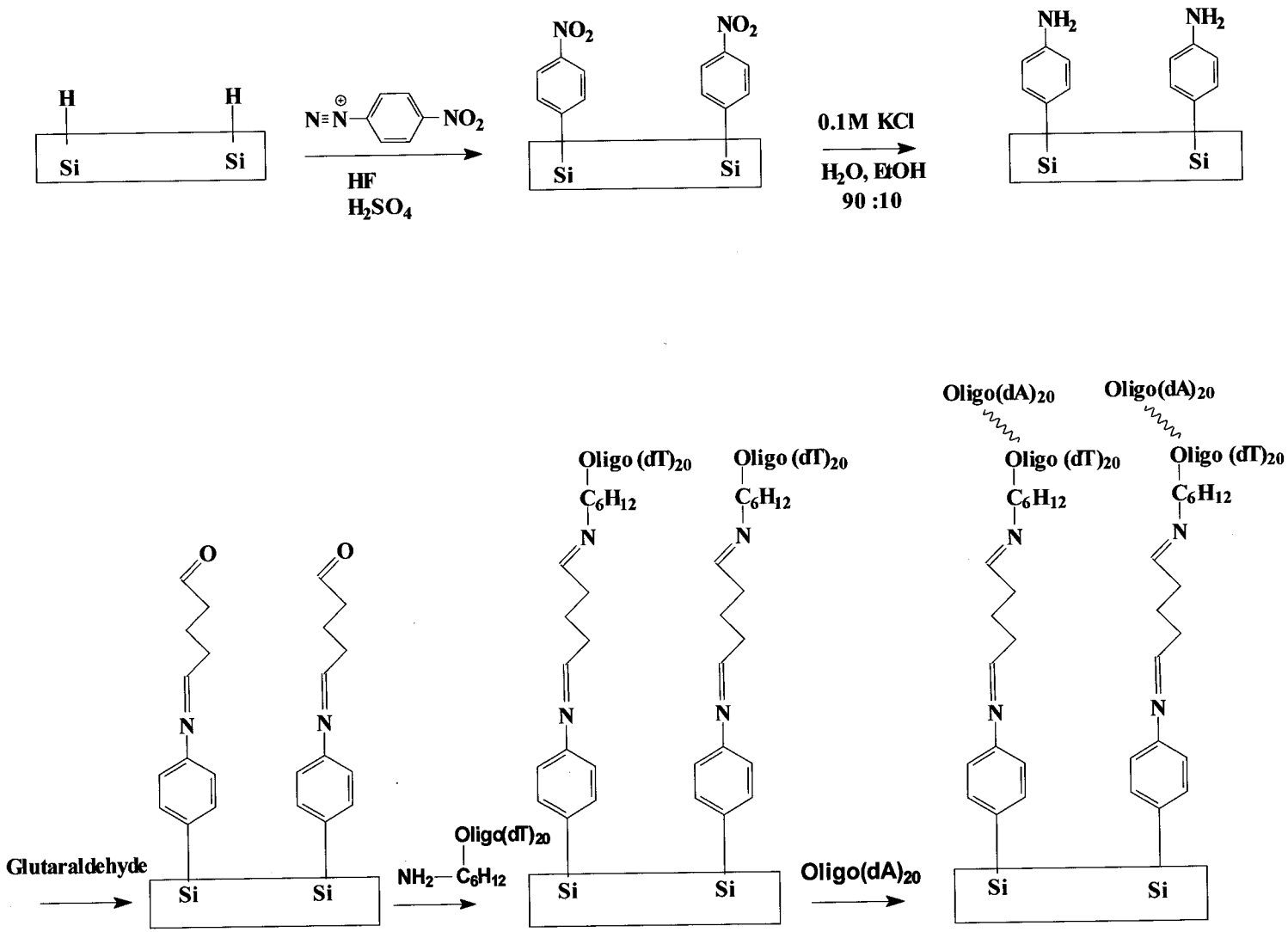

Scheme 1.1 Silicon functionalization, DNA immobilization and hybridization

1.1 Biosensors

Biosensors are small devices composed of two elements:

(*i*) a biological component, such as enzymes, antibodies or single stranded DNA used as probe layers, and (*ii*) a transducer such as a semiconductor, which converts the biological response into a measurable signal. Depending on the type of transduction, this signal can correspond to a variation in current, frequency, or fluorescence [27] (Figure 1.1).

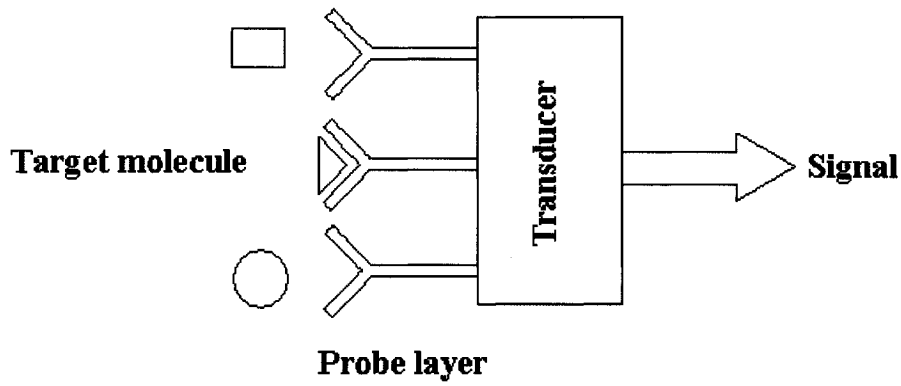

Figure 1.1 Biosensor components

One of the major interests in the field of biotechnology is developing DNA biosensors for genetic disease diagnostics and obtaining sequence-specific information. DNA biosensors commonly rely on the immobilization of single strand DNA (ssDNA) as a probe layer onto a solid surface and the detection of the complementary strand (target) upon duplex formation.

There are different types of DNA biosensor designs depending on the nature of the detection signal. They can be generally characterized as either direct or indirect detection devices. For example, fiber-optic DNA biosensors operate by attachment of ssDNA at the end of the fiber and observing the fluorescence changes upon double strand

DNA formation, resulting from the presence of a fluorescent label. These types of sensors require introduction of labels to make detection possible, and are referred to as indirect methods [28].

The quartz crystal microbalance (QCM) is another type of DNA biosensor, which is a device sensitive to mass variation during the recognition event. This is a direct (label-free) detection approach, which involves an oscillating crystal with a DNA probe immobilized on its surface. As the hybridization process proceeds, the increase in mass causes a decrease of the quartz transducer's oscillating frequency [29,30].

Another interesting detection approach uses electrochemical DNA biosensors, which can provide for either direct or indirect detection of specific DNA sequences with high sensitivity. The hybridization reaction can be readily detected by changes in electrochemical parameters such as conductivity, capacitance, and impedance (direct methods), or currents associated to an added redox-active indicator (indirect method) [1,2,31,32].

A successful biosensor must be highly specific and sensitive for the purpose of analysis, the response should be accurate, precise, rapid, and ideally, the complete biosensor should be small, cheap and portable. These analytical devices should also be able to provide results in a very short time using a very small amount of sample. The final aim of these micro-devices is to use direct (label-free) methods to avoid any pre-treatment, avoid any unwanted reaction of the sample with the attached labels, and allow for the possibility of *in-situ* monitoring.

II. Background

2.1 Nucleic Acid Chemistry

Nucleic acids are macromolecules of high molecular weight consisting of nucleotide units. The two types of nucleic acids are deoxyribonucleic acid (DNA), and ribonucleic acid (RNA), which store and express all the necessary information for building and maintaining life. Each nucleotide contains a nitrogenous base, a pentose sugar, and a phosphate group. The nucleic acid backbone is formed of sugars that are linked by phosphate groups through the connection of the 3'-hydroxyl group of one sugar to the 5'-hydroxyl group on the neighboring sugar. The direction of the overall sequence is written from the 5' to 3' end [33].

2.1.1 Nucleic acid bases

The nucleotides that exist in living cells are derivatives of the heterocyclic basic compounds, purines and pyrimidines. The pyrimidines are six-membered cyclic rings with two nitrogen atoms and four carbon atoms, while purines are formed from the fusion of an imidazole ring to a pyrimidine ring. The pyrimidine bases are cytosine (C), uracil (U), and thymine (T), and the purine bases are adenine (A), and guanine (G) (Figure 2.1). Both DNA and RNA are composed of the same purine bases, while the pyrimidine bases differ in DNA and RNA, where uracil is found in RNA instead of thymine in DNA.

Pyrimidine bases

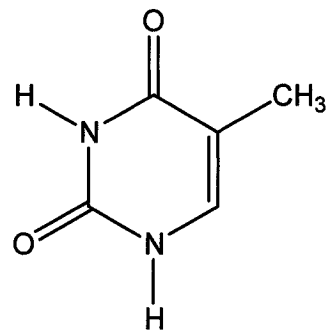

Thymine (T)

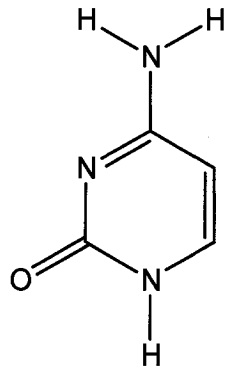

Cytosine (C)

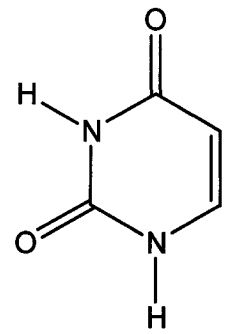

Uracil (U)

Purine bases

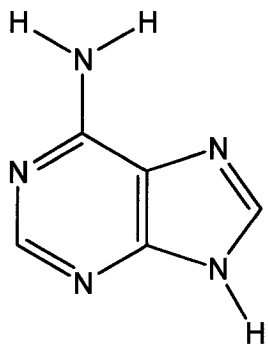

Adenine (A)

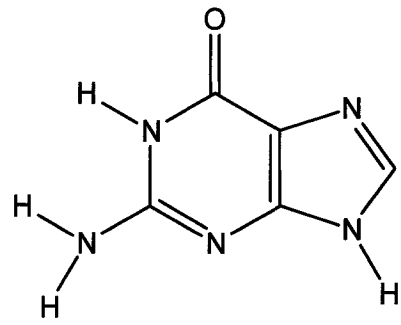

Guanine (G)

Figure 2.1 Structure of pyrimidine and purine bases

2.1.2 Pentose sugar

There are two types of pentose sugars forming the nucleic acid structures. Deoxyribose (D-2-deoxyribofuranose) found in DNA lacks the hydroxyl group in the 2-position that is present in ribose (D-ribofuranose) found in RNA. This small difference in

the pentose sugar affects the chemistry and the structure of the nucleic acids, hence the difference in their name (Figure 2.2) [33].

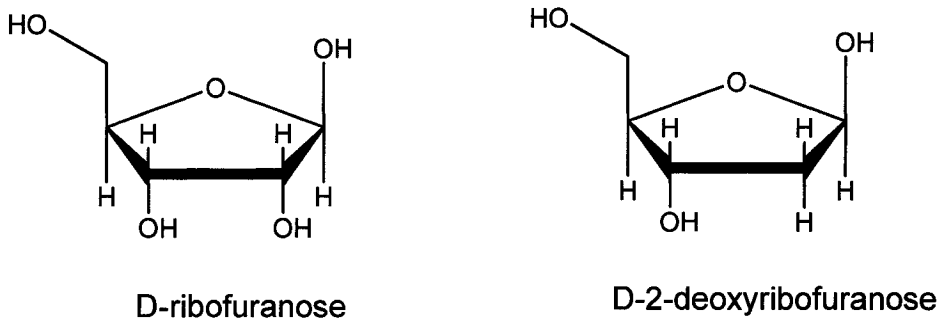

Figure 2.2 Pentose sugar structures

2.1.3 Phosphate group

Phosphate groups act to attach nucleoside units together through the phosphodiester bond between the 5'-phosphate group from one unit and the 3'- hydroxyl group of the next nucleotide sugar (Figure 2.3).

It is noteworthy to point out that the nucleosides are covalently linked to the C1' position of the sugar for each of the four DNA bases. Nucleosides differ from nucleotides in that they lack the phosphate group [33].

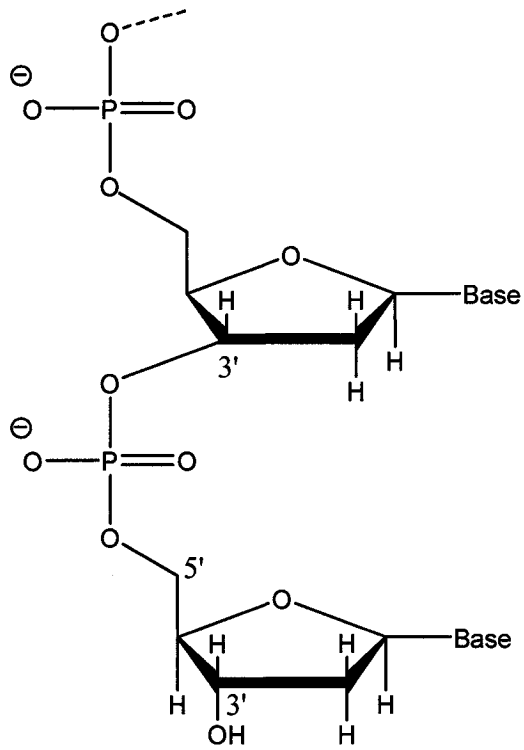

Figure 2.3 Attachement of oligonucleotides *via* a phosphate group

2.1.4 DNA duplex structure

Watson and Crick proposed the helical secondary structure of DNA chains as deduced from X-ray diffraction measurements in 1953 [34]. In this structure, a double helix with two oligonucleotide chains oriented in opposite directions is formed. The two single strands bind together through hydrogen bonding of the base pairs. Guanine binds specifically to cytosine through three hydrogen bonds, and adenine binds specifically to thymine through two hydrogen bonds (Figure 2.5). These hydrogen bonds are responsible for the stability of the duplex. Other forces stabilizing the structure of the duplex consist of base stacking forces, which are dipole-dipole interactions, van der Waals forces between adjacent bases, and hydrophobic interactions between purine and pyrimidine bases. However, electrostatic repulsion due to the negatively charged phosphate groups

forming the backbone contribute a degree of instability to the helix [35]. In the helical structure, bases are inside the helix, while the phosphate and deoxyribose groups occupy the exterior of the helix. The diameter of the helix is 20 Å and the distance between two adjacent base pairs is 3.4 Å [35]. Therefore, a double helix containing 10 base pairs will be 34 Å long (Figure 2.4). This DNA structure is known as B-DNA, which is the more common conformation of DNA. Other possible conformations of DNA are A-DNA and Z-DNA [35].

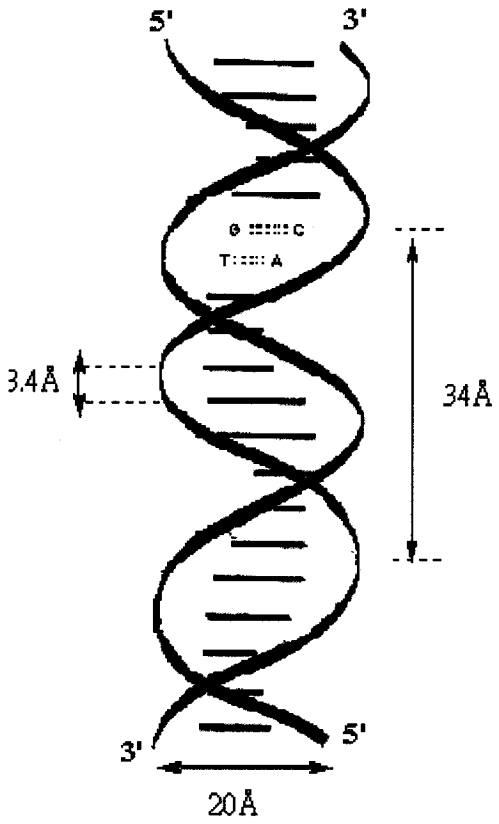

Figure 2.4 DNA duplex structure

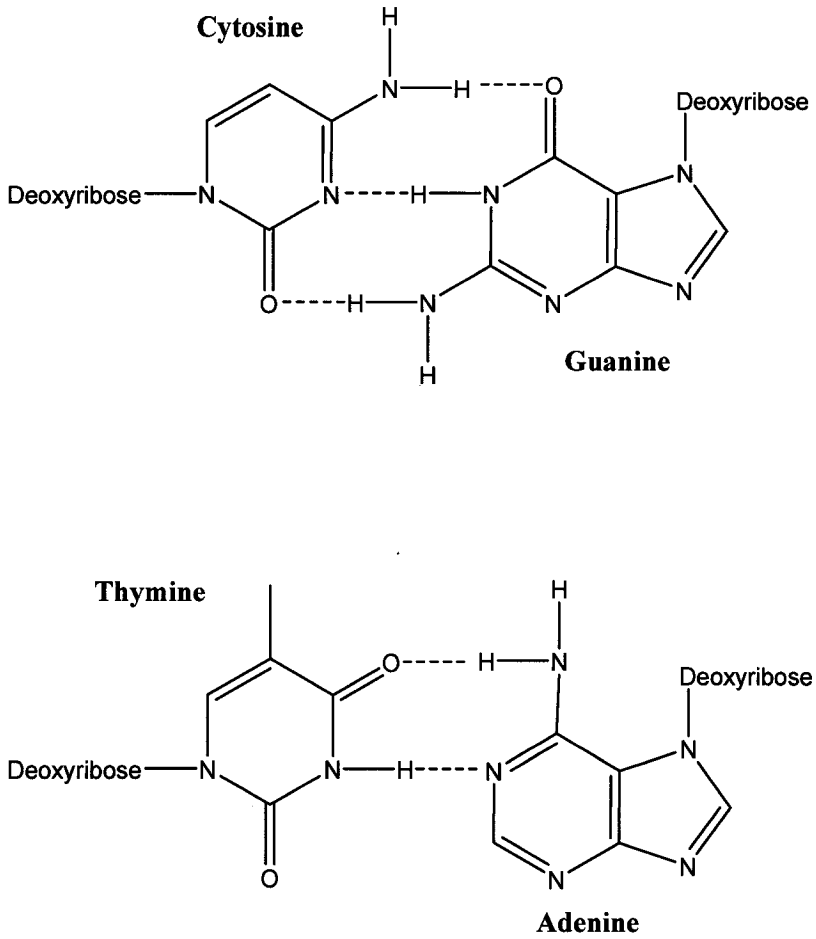

Figure 2.5 Base pair bonding

The difference between the three conformations of DNA depends on the sequence content, the ionic conditions, the conformation of the sugar (C_2'-endo or C_3'-endo), and the orientation of the base relative to the sugar (*syn* or *anti*) due to differences in torsion angle (χ) [36]. Z-DNA is longer and thinner than B-DNA, and is a left-handed helix with 12 base pairs per turn. The conformation of the pyrimidine bases are C_2'-endo, the purine bases are C_3'-endo, and the orientation of the purines and pyrimidines are *syn* and *anti*, respectively (Figure 2.6) [36].

A-DNA is wider than B-DNA and forms a right-handed helix similar to B-DNA. A-DNA is found when the concentration of cations is high and possesses 11 base pairs per turn. The conformation of the sugar in this form of DNA is C_3'-endo and the plane of bases is *anti* for both types of bases [36].

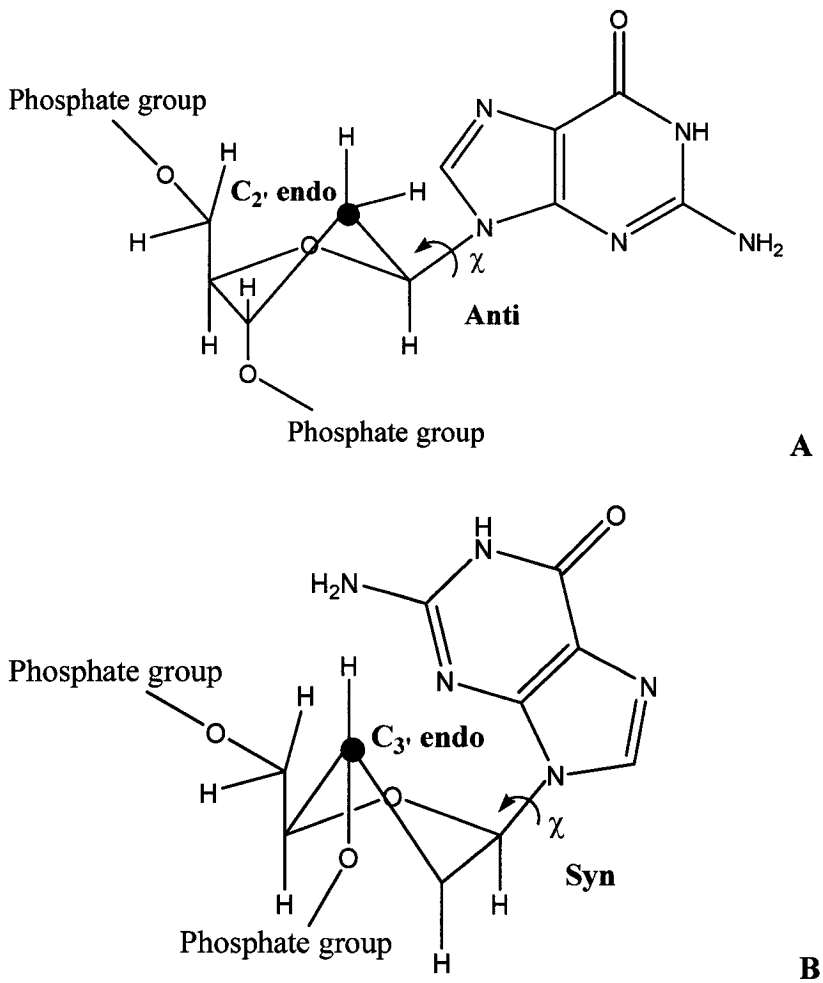

Figure 2.6 Conformation of the base-sugar linkage for guanine in B-DNA **(A)**, and guanine in Z-DNA **(B).**

2.2 Electrochemistry

2.2.1 Semiconductors

Semiconductors are materials that have electrical conductivity with magnitudes between that of conductors and insulators. In energy band diagrams of semiconductors, there is a valence band (V_B), which is defined as the energy levels occupied by electrons (bonding orbitals forming the band), the higher energy conduction band (C_B) formed from energy levels that are unoccupied by electrons (antibonding orbitals forming the band), and the band gap (E_g, energy difference between the valence and conduction bands, Fig 2.7) [37]. The band gap in semiconductors is usually less than 3 eV, such as for Si (Eg = 1.1 eV), InP (Eg = 1.3 eV), and CdS (Eg = 2.4 eV). If the band gap energy is greater than 3 eV, (such as diamond, Eg = 5.4 eV) the solid tends towards a more insulating behavior [37].

Semiconductors are generally characterized as:

1) Intrinsic semiconductors: Pure semiconductors without any defects or impurities in the structure.
2) Extrinsic semiconductors: Impure semiconductors containing impurities and defects (added intentionally or unintentionally) [38].

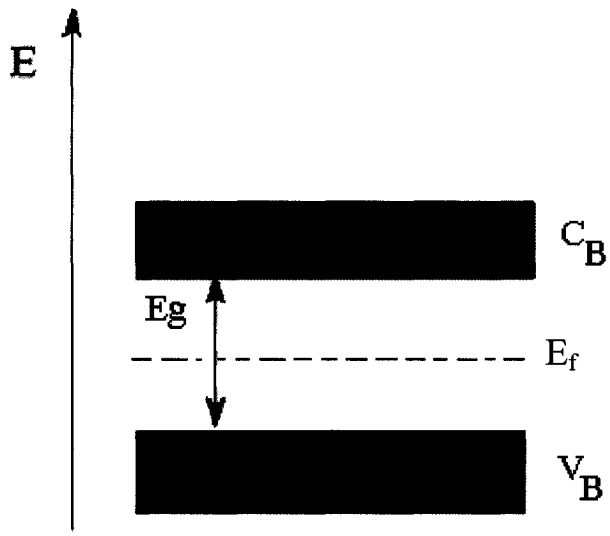

Figure 2.7 Energy band structure of an intrinsic semiconductor

In an intrinsic semiconductor, when an electron is promoted from the valence band to the conduction band, a hole or positive charge is left behind in the valence band. Movement of electrons in the conduction band, or holes in the valence band, produces conductivity. Electron promotion can occur through thermal or photon excitation [37].

2.2.2 Fermi level

The Fermi level (E_f in Figure 2.7) is defined as the energy at which the probability of occupation by electrons is equal to one-half. It also represents the average energy of species (electrons and holes) that can conduct electricity [37].

In an intrinsic semiconductor the Fermi level lies in the middle of the band gap, between the conduction band and valence band. On the other hand, in an extrinsic

semiconductor, the position of the Fermi level is different and depends on the type of impurities and defects that are present [37].

2.2.3 Doping

The process of intentionally adding impurities in the structure (crystal lattice) of semiconductors, for the purpose of controlling their conductivity, is called doping. By doping, it is possible to convert an insulator with a large band gap into a semiconductor. Depending on the chemical nature of the impurities added, semiconductor materials of two electrically different types can be produced; (*i*) electron-rich semiconductors called n-type, where 'n' stands for negative, or (*ii*) electron-poor semiconductors called p-type, where 'p' stands for positive [37].

2.2.3.1 N-type semiconductor

N-type behavior is induced by the addition of donor impurities having approximately the same size as the host semiconductor atoms, but with more valence electrons (such as doping the crystal structure of silicon with arsenic or phosphorus). The energy level of the extra electron associated with the donor is then located under the conduction band, and the electronic conductivity is controlled by excitation of electrons from these impurity energy levels to the conduction band (Figure 2.8A). In this type of semiconductor, electrons are the majority charge carriers [37].

2.2.3.2 P-type semiconductor

P-type behavior is induced by the addition of acceptor impurities that have a deficiency of valence electrons, compared to the host semiconductor atoms (such as

doping the crystal structure of silicon with boron). These electronically deficient atoms introduce unoccupied energy levels above the valence band, and hole conduction occurs by electron promotion from the valence band to the unoccupied acceptor levels (Figure 2.8B). In p-type semiconductors, holes are the majority charge carriers [37].

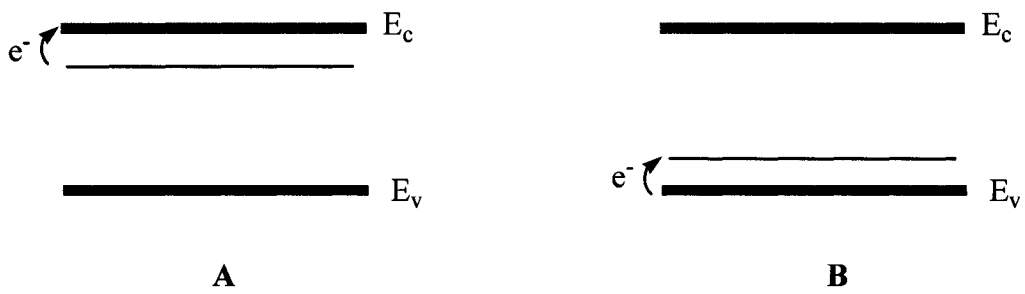

Figure 2.8 Energy band diagrams of different types of extrinsic semiconductors. **(A)** n-type, **(B)** p-type

2.2.4 Semiconductor-electrolyte interface

When a semiconductor is placed in contact with an electrolyte containing a redox couple, a double layer is formed at the semiconductor-electrolyte interface. Charges flow between the semiconductor and the electrolyte until an equilibrium is reached throughout the system, at which point the Fermi level in the semiconductor (E_f) is equal to the redox potential of the couple (Fermi energy associated to the redox couple) in the electrolyte, as illustrated in Figure 2.9.

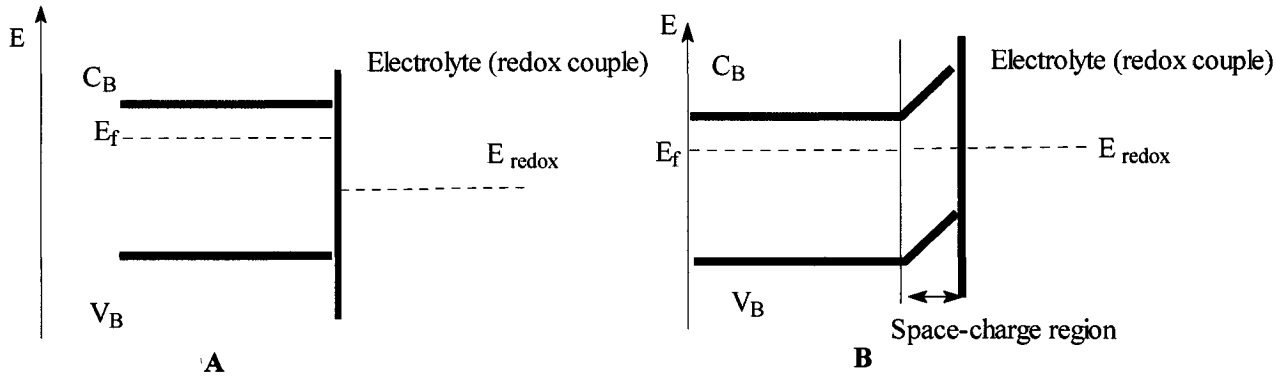

Figure 2.9 Energy bands at an n-type semiconductor-electrolyte interface, **(A)** before equilibrium, **(B)** after equilibrium

The equilibrium process produces a region within the semiconductor that is called the space-charge layer, where the charge distribution is different from that of the bulk material. This situation is represented by a bending of the bands within the semiconductor (at the semiconductor electrolyte interface), as illustrated in Figure 2.9B. It is possible to vary the degree of band bending in the semiconductor and effectively revert back to the situation illustrated in Figure 2.9A, referred to as the flat-band condition, by the external application of an appropriate potential to the semiconductor. The specific external potential that needs to be applied to exactly cancel out the band bending is called the flat band potential, V_{fb} [38]. The relationship between the space-charge density, and the existing electrical potential at the surface is given by Poisson's equation:

$$d^2\varphi/d^2x = \rho(x)/\varepsilon\varepsilon_o \qquad \textbf{[2.1]}$$

where φ is potential, ρ is the space-charge density , ε is the dielectric constant of the semiconductor, ε_o is the permittivity of free space, and x is the distance from the interface [38].

2.2.5 Impedance theory

Impedance (Z) is the alternating current (ac) analogue of resistance (R) associated with direct current (dc) measurements. When a dc potential (V) is applied to electronic circuitry, pure resistors (R) are observed to influence the passage of current (I) as described by:

$$V = RI \qquad [2.2]$$

When an ac potential (non-zero frequency) is applied, other elements such as capacitors and inductors influence the flow of current. These elements impact on the magnitude and phase of ac current as given by the complex form of Ohm's law:

$$\tilde{V} = Z\tilde{I} \qquad [2.3]$$

In ac theory the current and voltage are described by sinusoidal equations. The current sine wave can be expressed as:

$$\tilde{I} = I_o \sin(\omega t + \phi) \qquad [2.4]$$

where I is the ac current, I_o is the maximum amplitude of the ac current, ω is the angular frequency ($2\pi f$, f = frequency in Hz), t is time and ϕ is the phase angle. The ac voltage is given similarly by:

$$\tilde{V} = V_o \sin \omega t \qquad [2.5]$$

Figure 2.10 represents a typical plot of applied ac voltage across a circuit resulting in an ac current wave. In this diagram the voltage and current wave differ in amplitude as well as in phase. It is noteworthy to point out that current and voltage can be in phase ($\phi = 0$) or out of phase ($\phi = 90°$) [39].

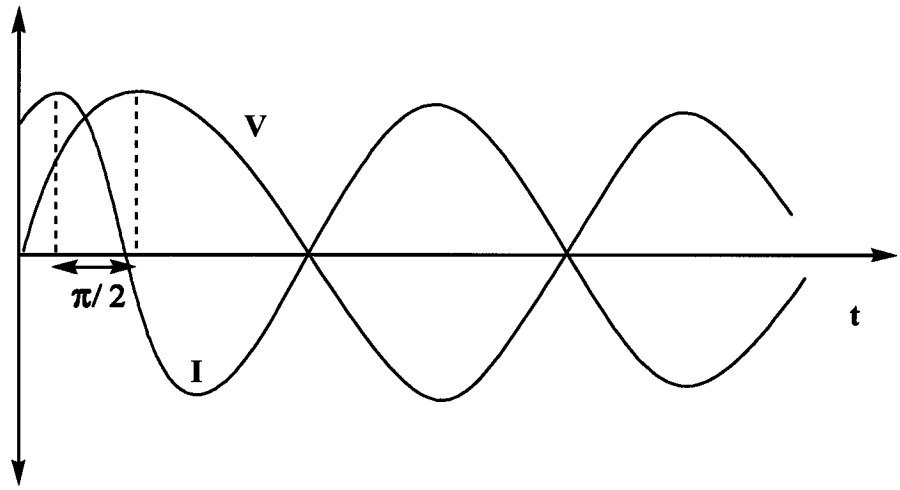

Figure 2.10 ac wave form for an applied potential and the resultant current

The alternating voltage and current can be defined as the sum of real and imaginary components:

$$Z = \frac{\tilde{V}}{\tilde{I}} = \frac{V_r + jV_i}{I_r + jI_i} \qquad \textbf{[2.6]}$$

where j is the square root of –1. By multiplying equation [2.6] by 1, where

$$1 = \frac{I_r - jI_i}{I_r - jI_i} \qquad \textbf{[2.7]}$$

the overall equation is expressed as:

$$Z = \frac{I_r V_r + I_i V_i}{I_r^2 + I_i^2} + j\frac{V_i I_r - V_r I_i}{I_r^2 + I_i^2} \qquad \textbf{[2.8]}$$

where the real part (Z_r) and the imaginary part (Z_i) of the overall impedance are resolved:

$$Z = Z_r + jZ_i \qquad \textbf{[2.9]}$$

The absolute magnitude of the impedance can be expressed as:

$$Z^2 = Z_r^2 + Z_i^2 \qquad [2.10]$$

and the phase angle is given by [39]

$$\tan\phi = \frac{Z_i}{Z_r} \qquad [2.11]$$

2.2.6 Equivalent circuit of EIS (Electrolyte/Insulator/Semiconductor) structures

The system used in this work for sensing purposes consists of a semiconductor (phosphorous-doped n-type silicon), which is used as a working electrode in electrolytic media for surface modifications. The organic films with which the electrode surface is modified, impart an insulating behavior that prevents the transfer of electrons between the electrolyte and the semiconductor. This EIS structure can be represented by an equivalent electrical circuit as shown in Figure 2.11 [39].

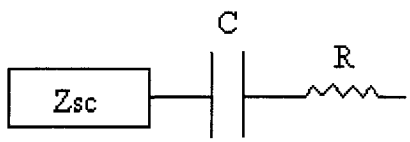

Figure 2.11 Equivalent model of an EIS structure

In this model, R is the resistance between the working electrode and reference electrode (resistance due to the electrolyte), Zsc is the impedance of the semiconductor and the capacitance, C, can be attributed to the double layer at the interface and to the presence of added insulating layers. Therefore measurements of capacitance can provide information on desorption and adsorption phenomenon, and film formation processes at an electrode surface. Each chemical modification at the semiconductor surface introduces changes

(thickness, dielectric constant of added insulating layers) in the overall equivalent circuit capacitance, as given by [38]:

$$C = \varepsilon\varepsilon_o A / d \qquad \textbf{[2.12]}$$

where ε_o is the permittivity of free space, ε is the dielectric constant of the insulating material, A is the surface area of the working electrode, and d is the thickness of the dielectric. Any changes in this capacitance are then reflected by changes in the out of phase impedance, according to the following equation [39]:

$$Z_i = 1/\omega C \qquad \textbf{[2.13]}$$

where ω is the angular frequency of the applied ac voltage, as described in the section on impedance [39].

2.2.7 Impedance measurements and determination of the flat band potential (V_{fb})

As described previously, the Fermi energy level can be varied (made more positive or more negative) by applying an external electrical potential to the semiconductor. By varying this externally applied potential, three distinct regimes can be identified, which are illustrated in Figure 2.12.

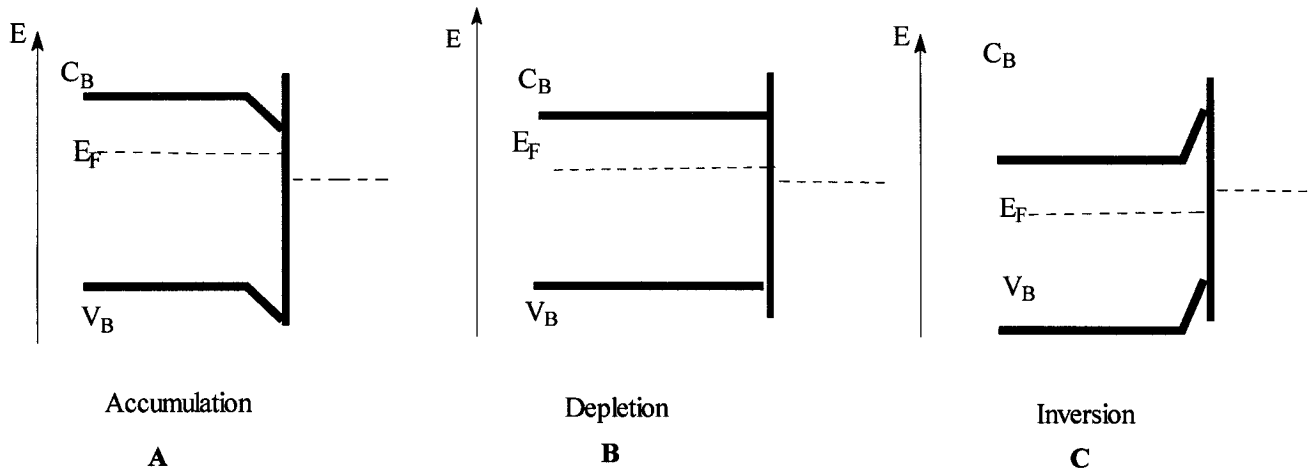

Figure 2.12 Band bending in the n-type semiconductor

2.2.7.1 Accumulation regime

When applying a negative potential (more negative than the flat-band potential, V_{fb}), the majority of charge (electrons) flows from the bulk toward the semiconductor interface, leading to an accumulation of negative charge in the space charge layer. This situation is shown in Figure 2.12A (bands bending downward at the interface), and is referred to as the accumulation regime [40].

2.2.7.2 Depletion regime

In going to intermediate, more positive, applied potentials (near the flat-band potential), the Fermi level moves downward toward the valence band causing gradual depletion of majority charge carriers in the space charge region. This situation is illustrated in Figure 2.12B and is referred to as the depletion regime [40].

2.2.7.3 Inversion regime

In going to even more positive potentials, an accumulation of minority charge carriers (holes) occurs in the space charge layer. This situation is shown in Figure 2.12C (bands bending upward at the interface, the inverse of the situation in Figure 2.12A), and is referred to as the inversion regime [40]. These changes in charge distribution at the semiconctor/insulator interface are readily monitored by measuring the out-of-phase impedance (Z_i) profile as the externally applied dc potential is varied to cover the three polarization regions: accumulation, depletion, and inversion regimes (as shown in Figure 2.13).

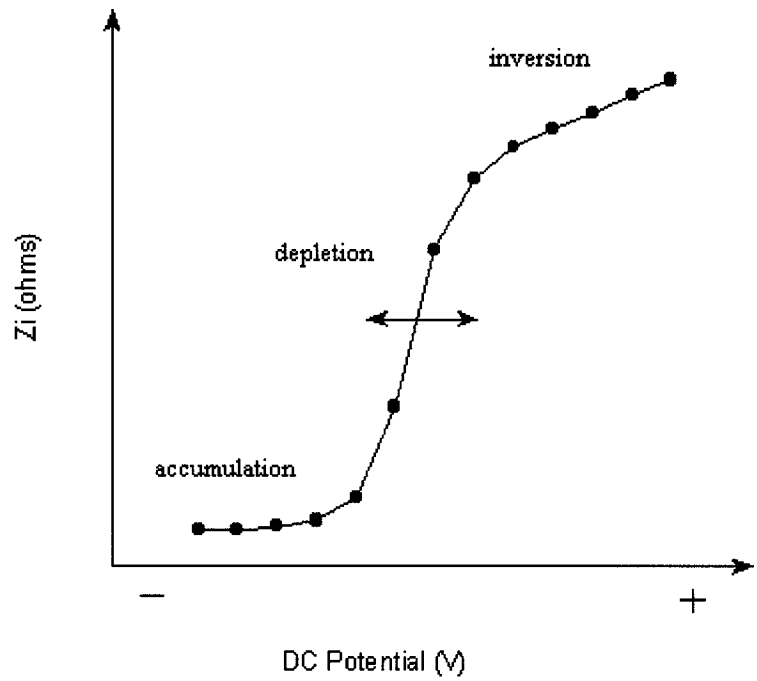

Figure 2.13 Impedance profile versus dc potential with different regimes

Extrapolation of the straight line of the depletion region (Figure 2.13) to the applied dc potential axis gives the flat-band potential (V_{fb}). The most common method to measure flat band potential is with the Mott-Schottky equation [37]:

$$1/C^2 = (2/\varepsilon\varepsilon_o q N_D A^2)(V-V_{fb} - kT/q) \qquad \textbf{[2.14]}$$

where q is the electronic charge, N_D is the dopant density per unit area, A is the area of the working electrode, ε is the relative permittivity of the semiconductor,ε_o is the permittivity of free space, V is the applied potential , V_{fb} is the flat band potential, k is the Boltzmann constant and T is the absolute temperature.

It should be stated that any modifications performed on the semiconductor surface (functionalization) leads to a change in the charge distribution of the space –charge layer causing a change in flat band potential. The change in the flat band potential shifts the impedance curves along the dc potential axis, which is the direct detection approach used in this study.

2.3 Scanning probe microscopy (SPM)

Scanning probe microscopy (SPM) is a surface characterization technique that provides information about surfaces at the nanoscale and allows one to visualize surfaces by scanning them with a sharp probe[41-44].

Scanning tunneling microscopy (STM) is the first family of probe microscopy, which is used to visualize surfaces by measuring electron tunneling between a conductive probe and surface. In 1986 Binnig and Rohrer obtained the Nobel prize in physics for invention a new member of the SPM family known as Atomic Force Microscope (AFM) or Scanning Force Microscope (SFM) [45].

2.3.1 Atomic Force Microscope (AFM)

In atomic force microscopy a constant force is applied between the probe and surface. A three dimensional image is obtained while the probe scans the surface. A piezoelectric scanner is responsible for the movement of the probe over the surface [46].

The main parts of an atomic force microscope are:

- Piezoelectric ceramic transducer
- Probes and cantilevers
- Optical detector (laser beam)
- Feedback loop control

2.3.1.1 Piezoelectric ceramic transducer

Two basic types of scanner exist in AFM: (*i*) the scanner that scans the sample under the tip and (*ii*) the tip that scans over the sample. The piezoelectric scanners are

ceramic PZT type materials (lead zirconate titanates). The scanner tube contains a thin-walled piezoelectric ceramic with electrodes placed at the internal and external faces of the tube. By applying a bias voltage between the inner and outer electrodes, the tube expands or contracts (*i.e.* it moves in the Z direction) but if the voltage is applied to only one of the outer electrodes, the tube will bend (*i.e.* it moves in the X and Y directions) [47].

2.3.1.2 Cantilever and tip

The main and most important part of the AFM is the tip, which is located at the end of the cantilever and interacts with the sample. The cantilever and tips are usually made from silicon or silicon nitride. The force (F) required to bend the cantilever is calculated by Hooke's law [46]:

$$F = -kd \qquad \textbf{[2.15]}$$

Where F is the force, k is the spring constant of the cantilever, and d is the cantilever's displacement. The minus sign in equation [2.15] indicates that the force acts in the opposite direction to the cantilever displacement.

2.3.1.3 Detection system

The cantilever movement can be recorded by several detection systems, the most common is based on an optical detector [46]. In this system a laser beam is reflected from the back of the AFM cantilever to a photodetector, a semiconductor device which converts light into an electrical signal. Any displacement of the tip and cantilever causes

a change in the reflected beam position on the photodetector, resulting in a change in the electrical signal (Figure 2.14) [46].

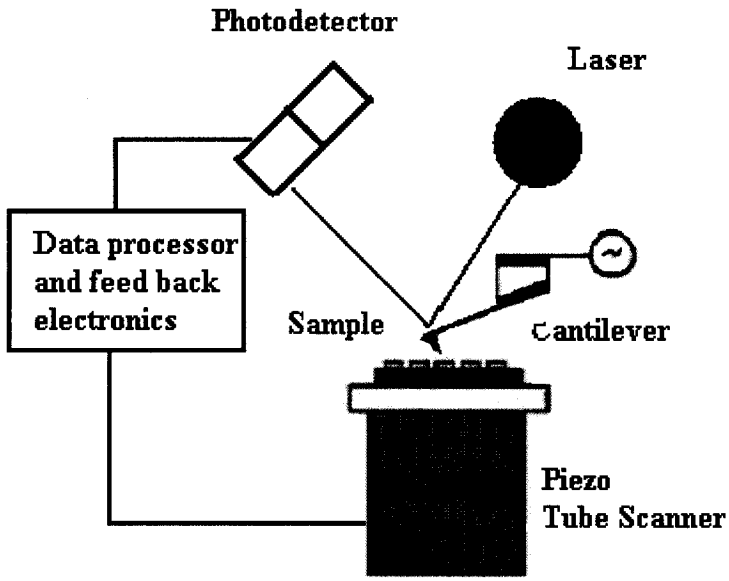

Figure 2.14 Laser beam deflection (detection method)

2.3.2.4 Feedback control loop

The voltage applied to the z-piezo element is controlled by a feedback loop system to keep the signal constant as the x and y piezo elements move the sample under the tip. The image is obtained by plotting the z-direction signal from the feedback loop versus the x and y directions [46].

2.3.2.5 Operation modes

Two main modes of operation are used to provide images in AFM: (*i*) contact mode and (*ii*) tapping mode.

2.3.2.5.1 Contact mode (deflection mode)

In the contact mode the tip scans the surface with a constant cantilever deflection, which is proportional to the force applied to the surface. In this mode the tip is in contact with the sample, therefore it is not ideal for probing soft surfaces since it can damage the sample.

2.3.2.5.2 Tapping mode (vibrational mode)

In tapping mode AFM, the cantilever is oscillated using a piezoelectric material as the sample is imaged. Due to the interactions of the tip with the surface, the amplitude and phase of the cantilever vibration changes during the scanning process. The advantage of this mode is that there is only intermittent contact with the surface, which greatly reduces the possibility of sample damage, especially for soft samples [46].

2.4 X-ray photoelectron spectroscopy (XPS)

X-ray photoelectron spectroscopy, also known as electron spectroscopy for chemical analysis (ESCA), is a surface sensitive characterization technique developed by Kai Seigbahn and his colleagues in the mid-1960's and used to determine the chemical composition of surfaces [48]. The fundamental principle of XPS involves irradiating a solid with monochromatic X-ray radiation of known energy (hν). When a photon with an energy of hν interacts with an atom on the sample surface, the electron is ejected from the atom and travels to the detector (Figure 2.15).

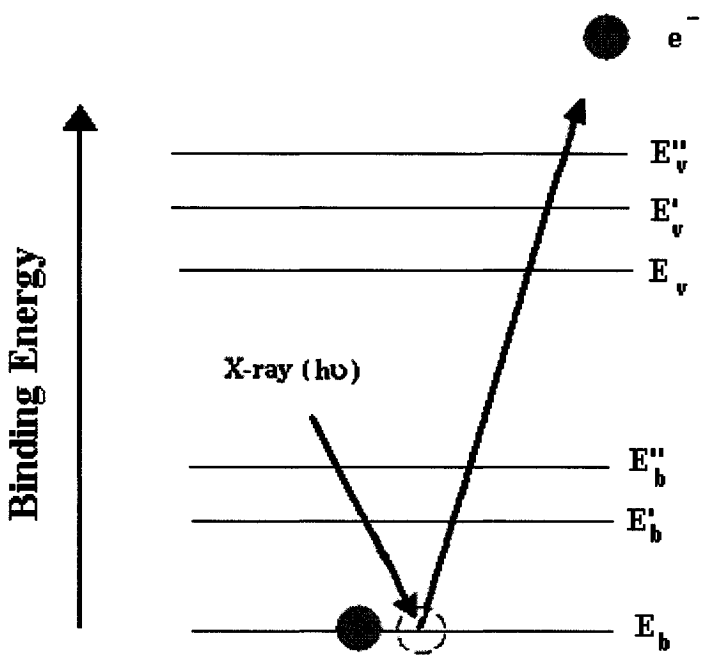

Figure 2.15 Schematic representation of XPS

In Figure 2.15 E_b, E_b', and E_b'' indicate energies of the inner shell K and L electrons of an atom and E_v, E_v', and E_v''indicate the energy levels of the valence electrons [49]. The

kinetic energy of the ejected electron can be calculated by the difference between the binding energy of the electron and the energy of the photon (equation 2.15).

$$E_k = h\nu - E_b - \phi_s \qquad \textbf{[2.15]}$$

where E_k is the photoelectron kinetic energy, E_b is the electron binding energy, $h\nu$ is the photon energy and ϕ_s is the work function. X-ray photoelectron spectroscopy can be used to quantitatively analyze solid surfaces and the oxidation state of elements (XPS can be used for all element except hydrogen), and can be used for the identification of functional groups. Quantitative analysis can be determined from peak height or peak area and chemical states can be determined from the measurement of peak position. The XPS measurement is usually easier to perform in the solid state with low-volatile samples. The samples must be stable under vacuum and not sensitive to damage by X-ray radiation [50].

III. Experimental section

3.1 Chemicals

4-Nitrobenzenediazonium tetrafluoroborate (97%), glutaraldehyde solution (grade II, 25%), and tetrabutyl ammonium hexafluorophosphate (TBAHFP) were purchased from Sigma-Aldrich. HF (50 %), H_2SO_4, acetonitrile (HPLC grade), and other solvents were purchased from Fisher. Ammonium fluoride (40%) was obtained from J.T. Baker. All non-labelled and fluorescein-labelled oligonucleotides ($dT_{(20)}$ and random probe sequences with amino linker $C_6H_{12}NH_2$ (noted as NH_2C_6 in the following text), and $dA_{(20)}$ target sequences) were purchased from Biocorp (Montreal) and were stored at -20°C. All solutions were prepared in distilled-deionized water, from a Milli-RX 20 Millipore system. All chemicals were used as received.

3.2 Apparatus

3.2.1 Silicon Substrates

Phosphorous-doped (5-10 Ω/cm) n-type Si (100) (Silicon Valley Microelectronics, USA), with a thickness of 300 μm and area of 1x1 cm^2, were used as individual substrates. These chips were taken from diced, 10 cm diameter polished wafers that were coated on the back with a gold/chromium layer (2000Å/500Å) providing an ohmic contact (Figure 3.1).

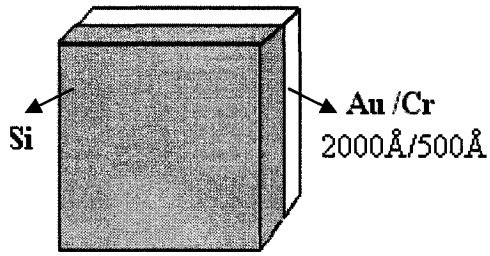

Figure 3.1 N-type Si (100) coated on the back with a gold/chromium layer

3.2.2 Electrochemical cell for functionalization of silicon

Electrochemical modification and impedance measurements were performed using a three-electrode cell, with the Si substrate acting as the working electrode, platinum foil as the counter electrode, and a standard saturated calomel electrode (SCE) (in aqueous solution), or Ag wire (in acetonitrile solution) as the reference electrode (Figure 3.2).

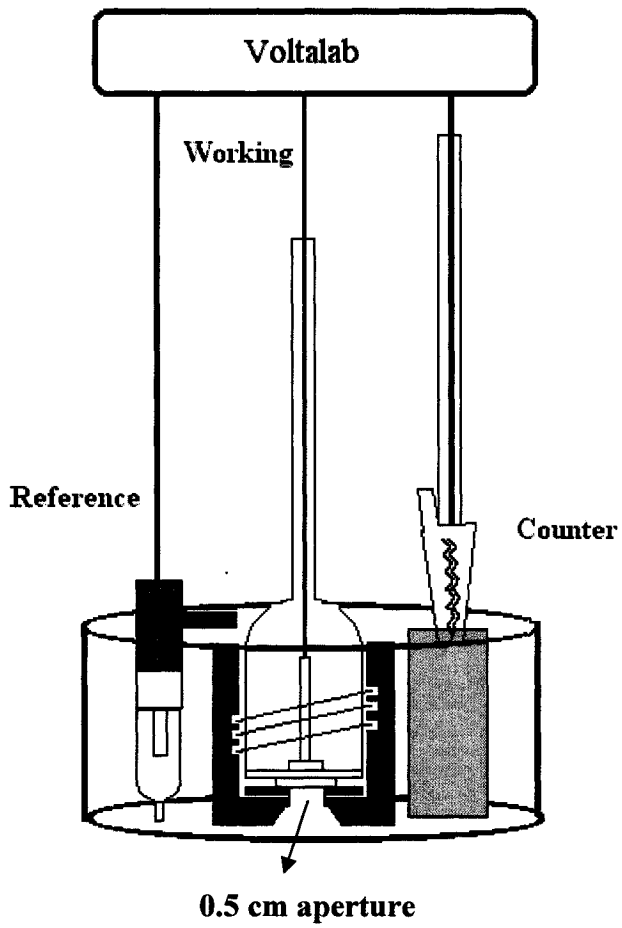

Figure 3.2 Schematic of the electrochemical cell for silicon functionalization

3.3 Procedures

3.3.1 Cleaning and etching procedures

Contaminants on the silicon chips were removed by immersion into trichloroethylene, acetone, and methanol (1 min each) and etched in a 50% HF solution (1 min) followed by treatment in buffered NH_4F 40% solution (6 min) to provide a hydrogen-terminated surface. These were then rinsed with distilled-deionized water and dried under nitrogen gas.

3.3.2 Silicon functionalization with diazonium salt

Cyclic voltammetry was performed using 2mM 4-nitrobenzenediazonium tetrafluoroborate solution with 2% HF and 0.1 M H_2SO_4 in aqueous media, or 2 mM 4-nitrobenzenediazonium tetrafluoroborate with 0.1 M tetrabutyl ammonium hexafluorophosphate (TBAHFP) in acetonitrile. All solutions were deoxygenated by bubbling nitrogen gas through the solution for 20 minutes before use. The nitro groups were then reduced to amino groups in 0.1M KCl (90:10 H_2O-EtOH) solution using cyclic voltammetry. For all cyclic voltammetric scans, the potential range was varied from -0.4V to -1.7 V , at a scan rate of 20 mV/sec. Contact between the working electrode and the electrolyte was limited to a circular area of 5 mm in diameter (corresponding to the aperture of a specially designed sample holder, Figure 3.2), in the center of the 1x1 cm^2 Si substrates. All cyclic voltammograms were obtained with a computer-controlled Voltalab electrochemical workstation (model PGZ 301 by Radiometer, Copenhagen). After the electrochemical modification, the chips were rinsed with distilled-deionized water and dried under a flow of nitrogen.

3.3.3 Glutaraldehyde treatment

The chips were subsequently functionalized with 40 μL of 25% glutaraldehyde solution for 15 minutes prior to immobilization of the oligonucleotide probes. The glutaraldehyde acts as a linker to attach the oligonucleotides to the surface.

3.3.4 Immobilization procedure

After treatment with glutaraldehyde, the chips were rinsed with distilled-deionized water and covered with 60 μL of aminolinker oligo $dT_{(20)}$ (0.02 μg /μL in 3 mM $NaHCO_3$ buffer solution pH = 8.4) for one hour. The modified chips were then treated with glycine (dipped in 0.1 M aqueous glycine solution for 20 min) to cap off any unreacted aldehyde groups remaining after probe immobilization.

3.3.5 Hybridization of oligonucleotide

The target $dA_{(20)}$ was diluted in hybridization buffer (1mM citrate solution pH = 8.5) to a final concentration of 2 ng/μL. 40 μL of this solution was placed on the chips for 2 h at 26°C, then the surface was washed with distilled-deionized water and dried with a stream of nitrogen gas.

3.3.6 Impedance measurement

A three-electrode setup described previously (Figure 3.2) was used to perform impedance measurements. A DC potential between -1.2 to 0.2 V, with a superimposed ac voltage of 10 mV amplitude at a frequency of 100 kHz, was applied to the working electrode. All measurement was performed in a 0.1 M NaCl electrolyte solution in a dark box using a Voltalab electrochemical workstation (model PGZ 301 by Radiometer, Copenhagen). The Voltamaster computer program (version 4.0) was used to calculate out-of-phase impedance (Zi) and the data was analyzed using Kalidagraph software.

3.3.7 Screen-printed electrodes (SPEs)

The carbon ink [electrogag 423 SS (Acheson, France)] was printed onto A5 (21 x 14.8 cm) polyester flexible sheets using a DEK 248 screen-printing machine (DEK, France). The polyester sheets with 16 electrode arrays were subsequently baked 10 minutes at 100 °C to dry the thermoplastic carbon ink [51] (Figure 3.3).

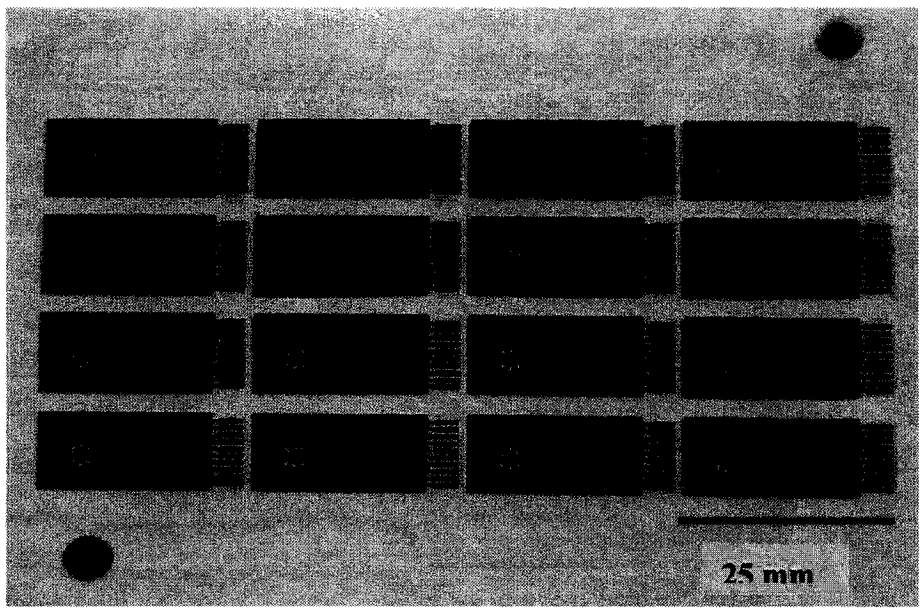

Figure 3.3 Screen-printed electrodes

3.3.8 Functionalization of SPEs with carbodiimide

The SPEs were functionalized with 40 μL of 0.1 M 1-(3-dimethylaminopropyl) ethylcarbodiimide hydrochloride (EDC) in 0.12 N HCl through chronoamperometry for 20 minutes. A potential of +2.2 V was applied to oxidize the carbon and generate carboxyl groups on the surface, which can react with the EDC. The electrodes were subsequently washed with distilled-deionized water and air dried.

3.3.9 Immobilization of oligonucleotide sequences (20mer & 200mer)

After functionalization, the SPEs were rinsed with distilled-deionized water and coated with 60 μL of aminolinker oligo $dT_{(20)}$ or oligo $dT_{(200)}$ (0.02 μg/μL in 0.1 M Na_2CO_3 buffer solution pH = 10.4) for one hour. The SPEs were subsequently covered with VBST (30mM Veronal buffer with 0.2M NaCl and 0.1% Tween, pH = 8.5) for 20 minutes. The electrodes were then immersed in VBS (30 mM Veronal buffer with 0.2M NaCl, pH = 8.5) for 20 minutes, rinsed with distilled-deionized water and air dried.

3.4 Characterization methods

3.4.1 Atomic force microscopy (AFM)

A Nanoscope IIIa AFM microscope (Digital Instruments, Santa Barbara, CA) was used to capture AFM images using the tapping mode in air at room temperature, with etched silicon cantilevers (RTESP NanoProbe, Veeco, Santa Barbara, CA) with a resonance frequency of ~300 kHz, a nominal spring constant of 20-80 N/m, and a tip radius of 10-12.5 nm. An oscillation amplitude of 175 mV and medium damping (~25%) were employed for these measurements. Contact mode topographic images were acquired in air using V-shaped, oxide-sharpened silicon nitride cantilevers (Digital Instruments) with a nominal spring constant of 0.58 N/m. Films were imaged with the minimum force required to keep the AFM tip in contact with the surface. The images were collected with high resolution (512 points per line) at a scan rate of 1-2 Hz. Contact mode AFM was used to produce holes in the surface. In this case, a set point voltage of 10 V with a high scan rate (59 Hz) was used to purposely scratch the surface layer.

3.4.2 Ellipsometry

Ellipsometry measurements were carried out with an I-Elli2000 imaging ellipsometer (Nanofilm Technology GmbH, Göttingen, Germany) equipped with a 50mW Nd:YAG laser with wavelength λ = 532 nm. Experiments were performed at an incident angle φ = 70.00° and a laser output of 1-2% with the analyzer and compensator set to 45.00°. To determine the optical thickness of the organic film at the surface, the

following values for n (refractive index) and k (extinction coefficient) were used: Si wafer as substrate (n = 4.15, k = 0.0449), polyaniline as model for the organic film (n = 1.247, k = 0.031). Ten measurements were performed per sample, each one taken at a different location on the same sample, and average overall thicknesses are reported for 3 samples following a single scan and for 3 samples following three scans.

3.4.3 X-ray photoelectron spectroscopy (XPS)

XPS measurements were performed on several chips following each of the electrochemical modification steps. They were analyzed using a VG 220iXL spectrometer using an Al X-ray source at 1486.6 eV. The pressure of the analysis chamber was 10^{-9} torr and the data was collected and analyzed using Casa XPS.

3.4.4 Fluorescence

Following the procedures outlined above in the experimental section on oligonucleotide immobilization and hybridization, immobilization of the probe layer through a glutaraldehyde-amino group linkage was verified using fluorescein-labelled (NH_2C_6)-dT(20) as an indicator. Hybridization to immobilized oligo dT(20), and alternately to random non-complementary (AGTCCATTGCAGTCCATTGC) probe sequences, was also tested using fluorescein-labelled oligo dA(20). The fluorescence images were obtained using a Genepix 4000B fluorescence microarray scanner. The images were obtained at a wavelength of 532 nm and the pixel size was set at 20 μm. The photomultiplier tube (PMT) voltage and focus were adjusted to 1000 V and 200 μm, respectively.

IV. Results and Discussion

4.1 Functionalization methods for silicon substrate

4.1.1 Electrochemical functionalization of silicon chips in aqueous media

The first step for chemical functionalization of etched n-type Si (100) chips was carried out using cyclic voltammetry in contact with an aqueous 2 mM tetrafluoroborate 4-nitrobenzene diazonium solution with 2% HF and 0.1 M H_2SO_4. The initial scan (Figure 4.1, curve 1) shows a broad and irreversible cathodic wave at around -1.3 V *vs* SCE, which upon subsequent scans gradually tends toward a flat, near zero cathodic current profile (Figure 4.1, curve 2) due to surface passivation. This reduction process of the diazonium moiety is illustrated in Scheme 4.1.

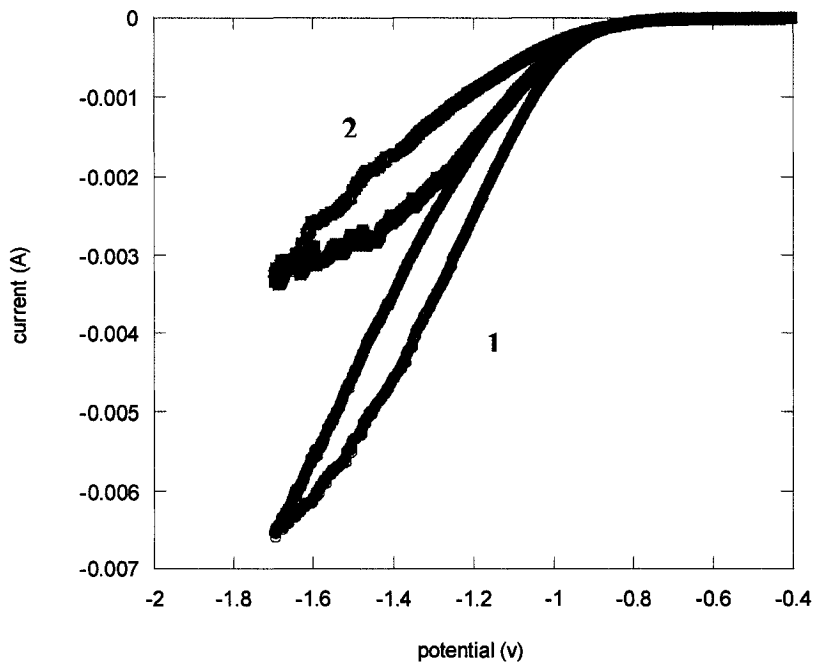

Figure 4.1 Cyclic voltammograms for the functionalization of Si (100) with $BF_4.N_2$ (C_6H_4)-NO_2 in aqueous media (curve 1 first scan, curve 2 second scan)

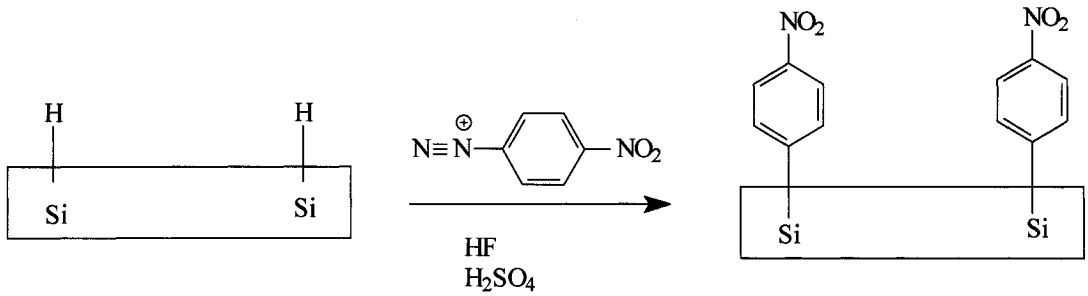

Scheme 4.1 Idealized electrochemical attachment of nitrophenyl groups to the Si surface

The next step in surface functionalization is the cyclic voltammetric reduction of nitro groups to amino groups using a 0.1M KCl, (90:10 H_2O-EtOH) solution (Figure 4.2). The reduction of the nitro groups is a six-electron reduction process, as described in Scheme 4.2 [52]. It should be noted however, that although these voltammetric steps are intended to accomplish an overall 6 e^- reduction of NO_2 to NH_2 [52], there have been reports focused on carbon surface modifications indicating that this reduction is only partial, resulting in a small fraction of NO_2 groups undergoing a 4 e^- reduction to form NHOH rather than NH_2 [16,23] . This aspect was further investigated herein by XPS measurements.

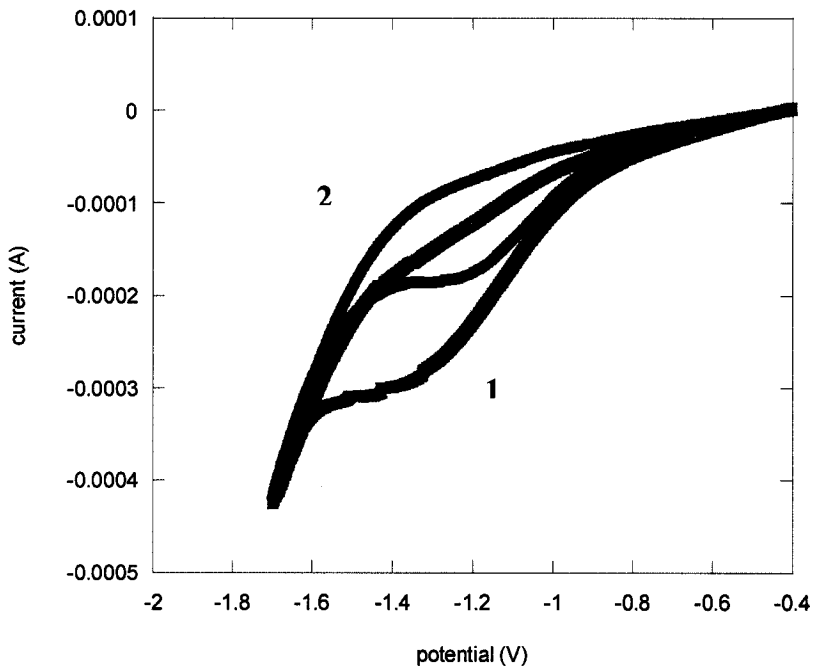

Figure 4.2 Cyclic voltammograms for the reduction of nitro groups to amino groups, (curve 1 first scan, curve 2 second scan)

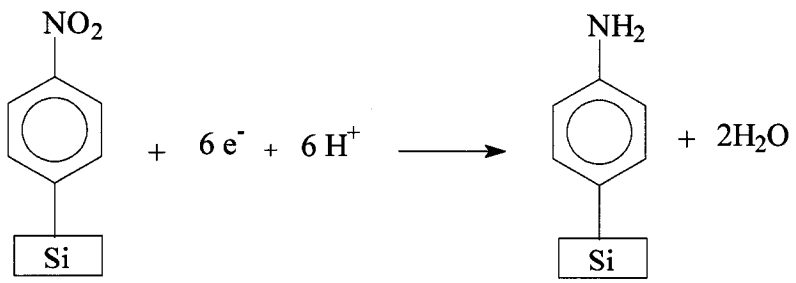

Scheme 4.2 Reduction of nitro groups to amino groups

4.1.2 Electrochemical functionalization of silicon in acetonitrile

Electrochemical functionalization was also carried out using the same diazonium salt in acetonitrile (2 mM concentration with 0.1 M tetrabutyl ammonium hexafluorophosphate as background electrolyte). Films formed in acetonitrile show a prominent reduction wave at approximately -0.6 V *vs* Ag (Figure 4.3). Comparing Figures 4.1 and 4.2 (initial functionalization and subsequent reduction of NO_2 to NH_2 in aqueous media) with Figures 4.3 and 4.4 (same two steps respectively, in acetonitrile), it is clear that the currents observed in water are *ca.* 2 orders of magnitude greater than those observed in acetonitrile for the initial aryl-nitro deposition, and *ca.* 1 order of magnitude greater for the reduction of NO_2 to NH_2. The reduction currents in the second voltammetric scan were always observed to be much less prominent in acetonitrile than in water. It is also important to note that gas bubbles evolve from the Si working electrode during the cyclic voltammetric scan in aqueous media, whereas no bubble evolution was observed in acetonitrile. As discussed in the following section on AFM measurements, this has a clear impact on the quality of films obtained from electrochemical functionalization in water versus those obtained in acetonitrile.

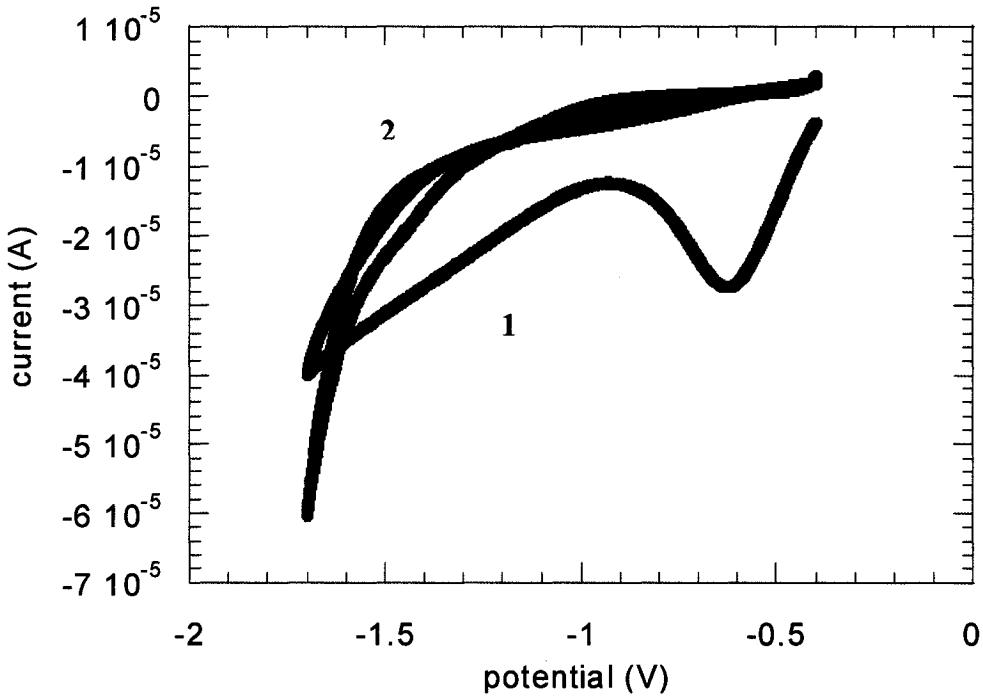

Figure 4.3 Cyclic voltammograms for the functionalization silicon with $BF_4.N_2$ (C_6H_4)-NO_2 in acetonitrile (curve 1 first scan, curve 2 second scan)

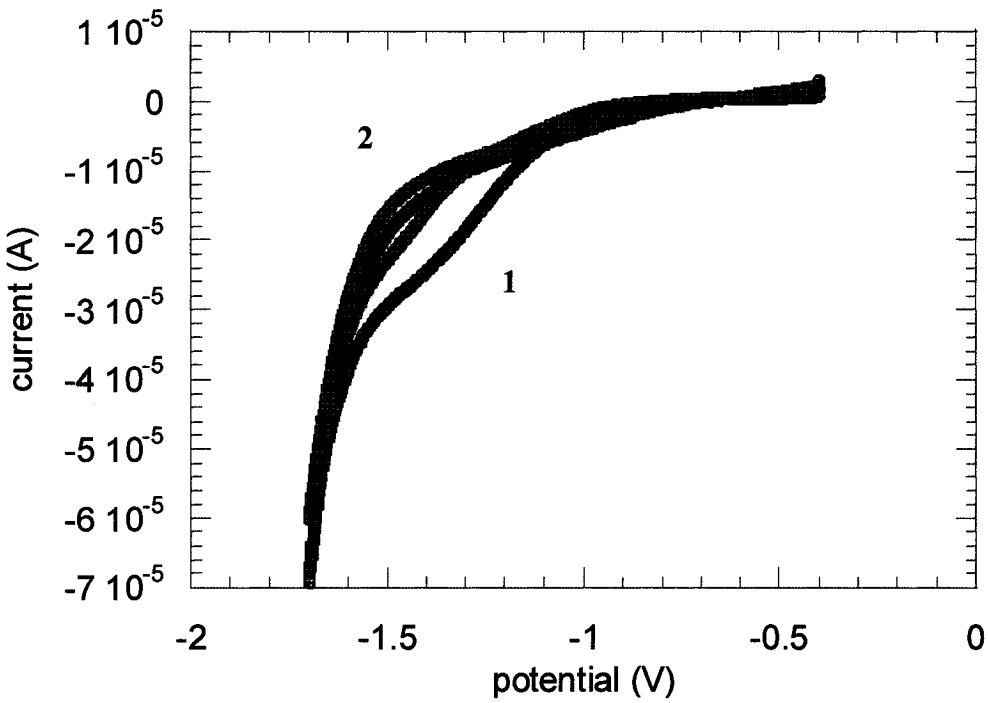

Figure 4.4 Cyclic voltammograms for the reduction of the nitro groups to amino groups in aqueous media, after initial functionalization in acetonitrile media (curve 1 first scan, curve 2 second scan)

4.2 Atomic force microscopy (AFM) images

Tapping mode AFM was used to investigate topographical changes at the silicon surface caused by the electrochemical modification. Figure 4.5A shows the AFM image of a Si substrate after the cleaning/etching procedure. Figure 4.5B shows an image of the resulting film (following 3 voltammetric scans for Ar-NO_2 film formation, and the NO_2 to NH_2 reduction step), which clearly shows the presence of micrometer-sized holes in the layer (the matter stripped from the surface (leaving the holes) appears to redeposit on top

of the layer at close proximity to the holes). Figure 4.5C clearly shows that these holes are not produced when films are formed in acetonitrile.

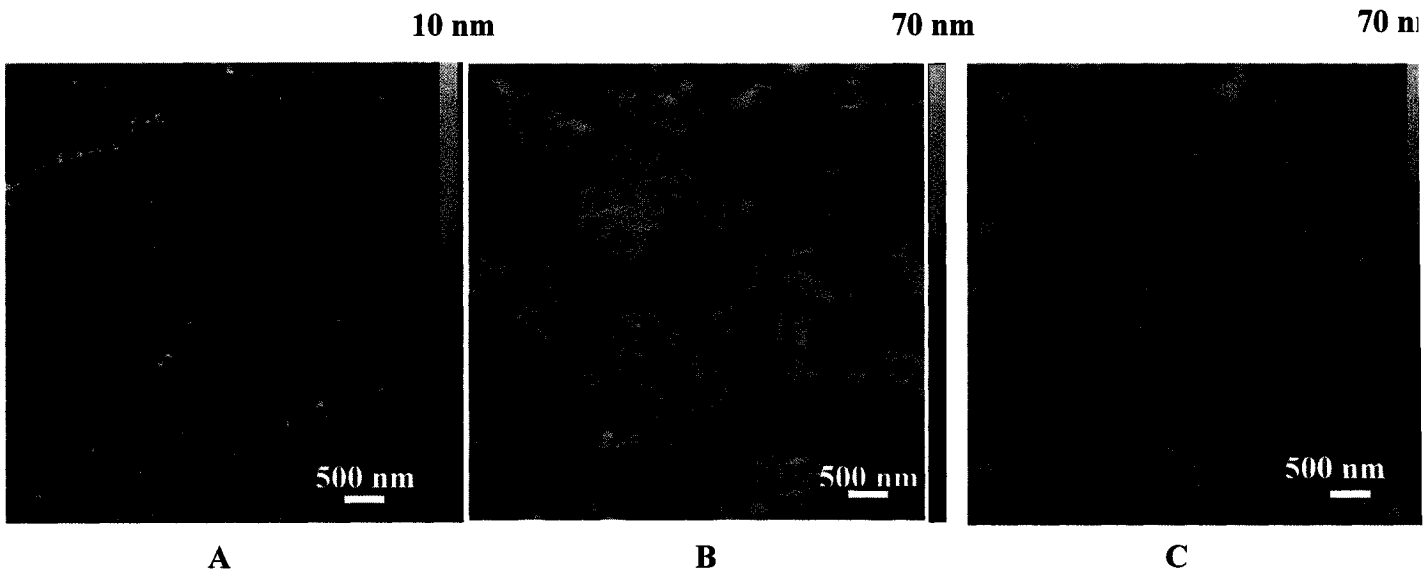

Figure 4.5 AFM tapping mode images of a Si (100) substrate before functionalization (**A**), after chemical functionalization in aqueous media (**B**), and after chemical functionalization in acetonitrile (**C**)

Film formation using this electrochemical approach proceeds *via* the generation of aryl radicals to form Si-Ar-NO_2 bonds (reactions 1, 2, & 3 in Scheme 4.3). As reaction 4 of Scheme 4.3 indicates, in aqueous media the formation of hydrogen molecules may also occur [15] (as reflected by evolution of gas bubbles at the working electrode during the electrochemical modification), yielding higher reduction currents. These observations, and the fact that uniform homogeneous, hole-free, films are obtained in acetonitrile, tend to indicate that the holes generated in aqueous media are indeed due to the reduction of water.

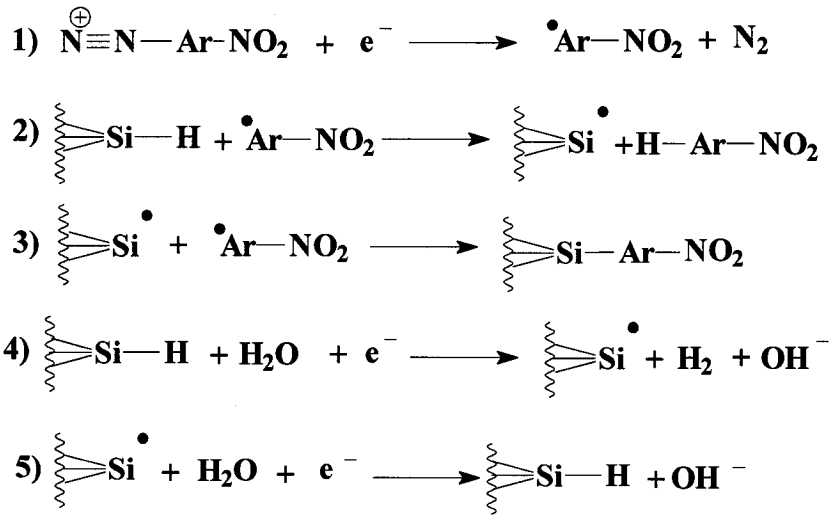

Scheme 4.3 Mechanism of film formation

4.3 Layer thickness measurements by AFM

To measure layer thicknesses, contact mode AFM was employed to produce holes in the deposited layers. After scratching the surface, using high applied force and fast scan rates, the AFM tip was withdrawn from the surface, zoomed out to a larger scan size, and re-engaged with minimum force (set point voltage = 1V). Layer thicknesses estimated from cross-sectional profiles of films obtained following 3 voltammetric scans for both reduction steps, whether the initial reduction step was performed in aqueous or acetonitrile media, were approximately 35 nm. The depth of holes produced by scratching the surface (Figure 4.6, blue line), was the same as that of holes attributed to the evolution of hydrogen bubbles in aqueous media (Figure 4.6 A, red line). It should be noted that this result, in addition to the fact that the AFM tips are typically damaged or broken upon insistent contact with the solid Si surface (providing a clear distinction

between Si surface and deposited organic film), indicates that these reported film thicknesses carry no contribution from scratching into the Si surface. Layers produced with a single scan were also examined and the thicknesses in this case were found to be approximately 5 ± 2 nm in aqueous solution, and 15 ± 2 nm in acetonitrile (Figure 4.7). These values are much greater than that of a monolayer, which would be approximately 7 Å thick[15].

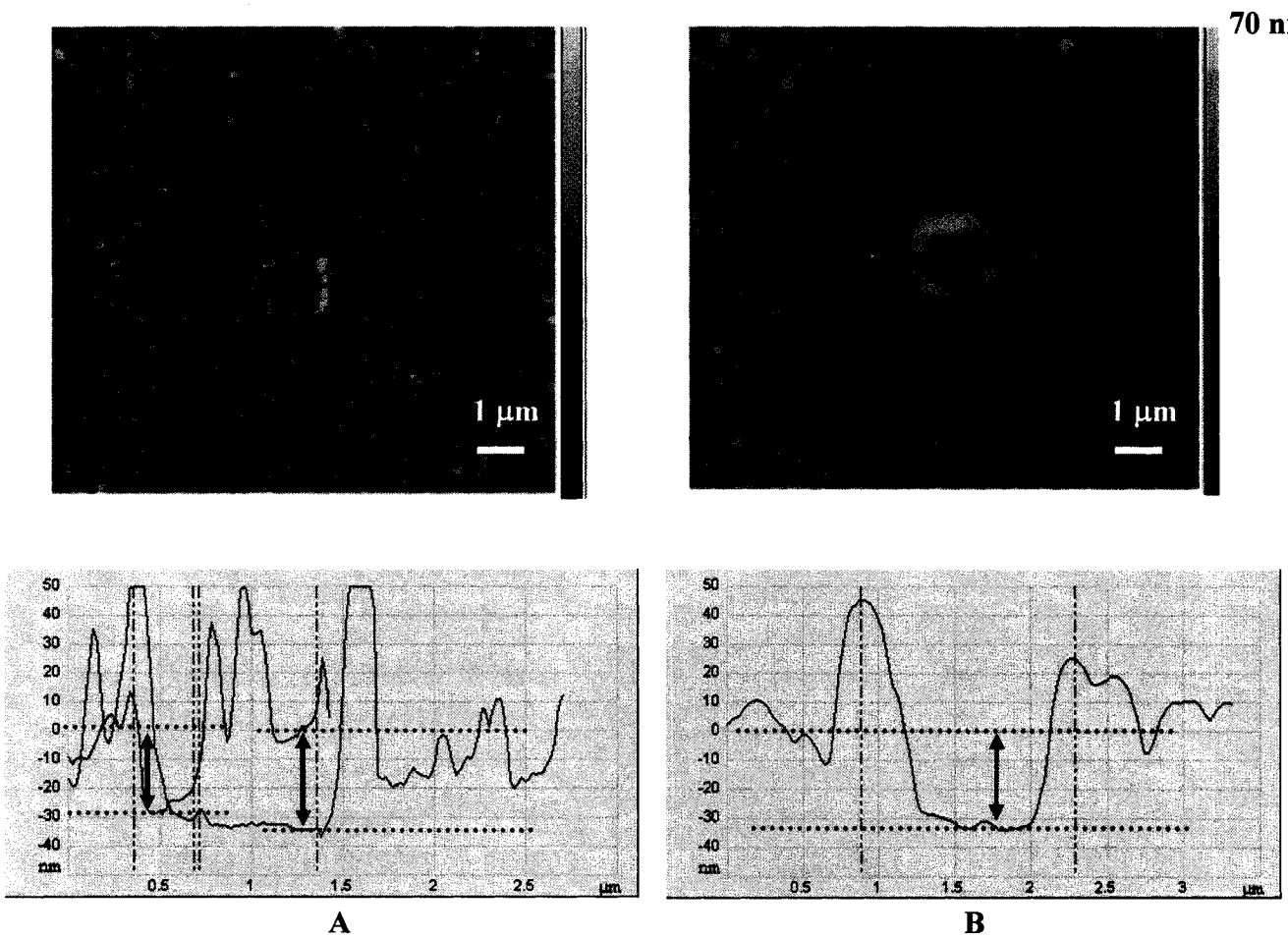

Figure 4.6 Thickness measurements using AFM contact mode of a silicon surface modified in aqueous solution **(A)** and in acetonitrile **(B)** following three cyclic voltammetric scans

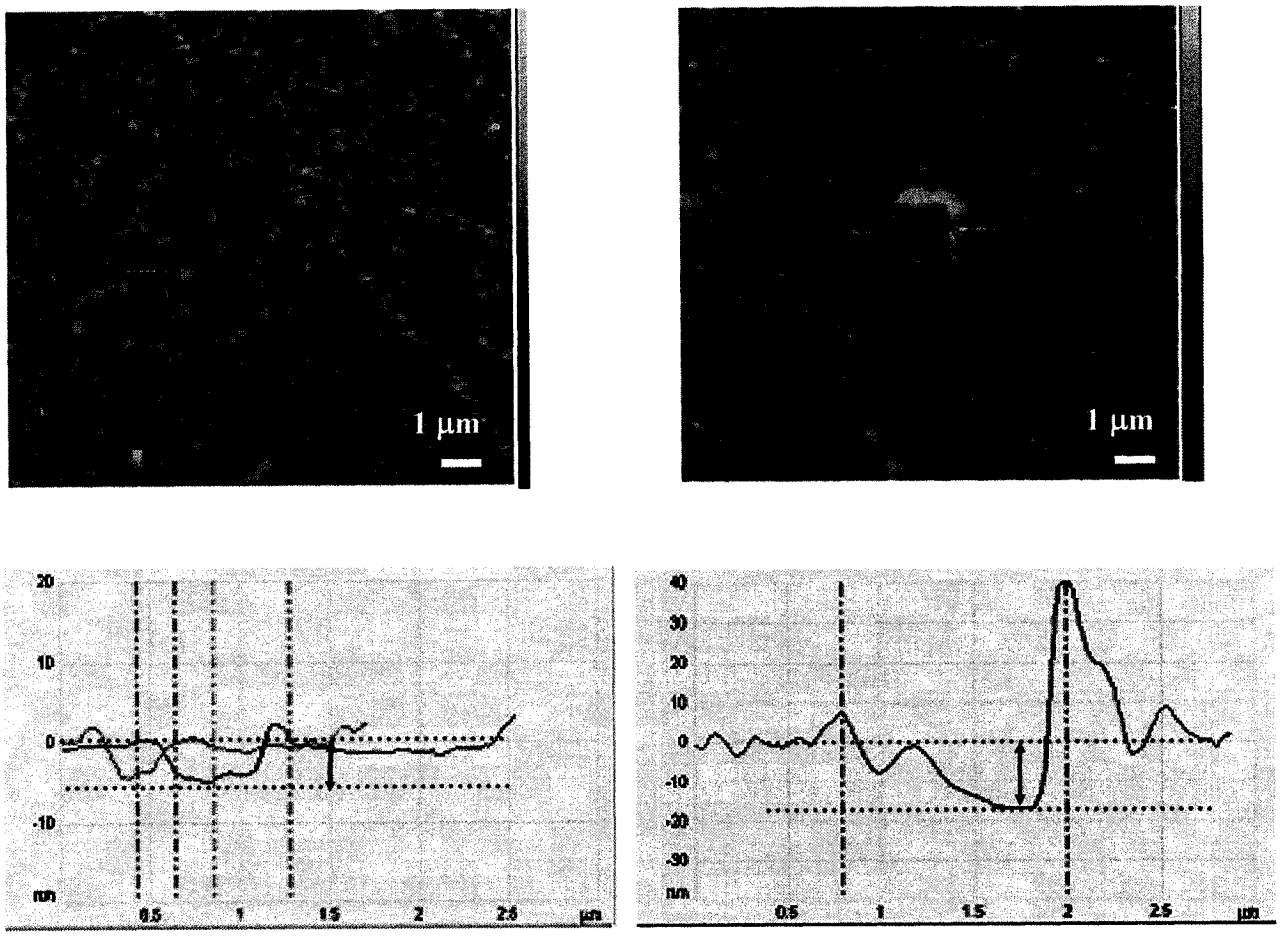

A B

Figure 4.7 Thickness measurements using AFM contact mode of silicon surface modified in aqueous solution **(A)**, and in acetonitrile **(B)** following a single cyclic voltammetric scan

Multilayer formation using this approach has been reported in the literature, and is explained by the mechanism shown in Scheme 4.4 where electrochemically generated aryl radicals attack the surface bound phenyl groups leading to the formation of multiple layers[53].

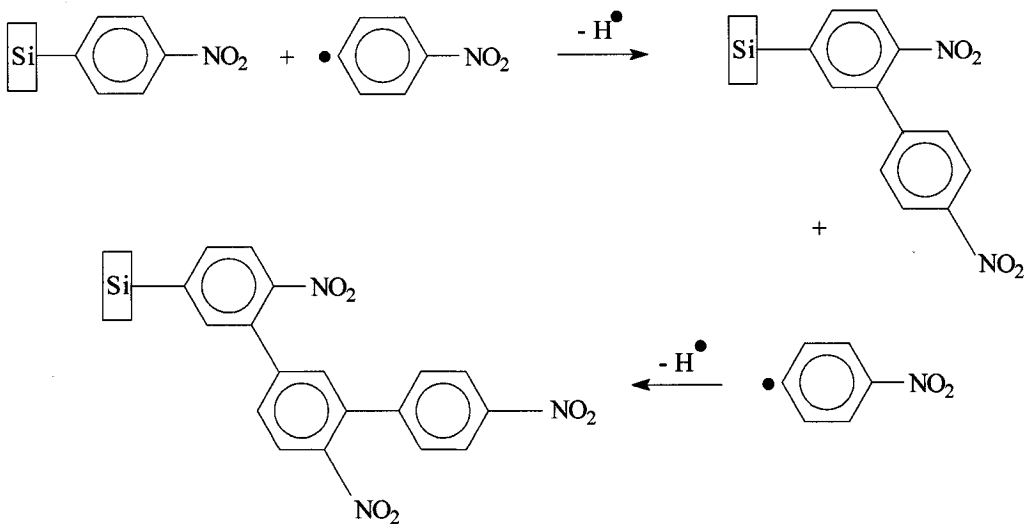

Scheme 4.4 Multilayer formation film *via* the attachment of aryl radicals to surface bound phenyl groups

4.4 Ellipsometry

Ellipsometry was used to further confirm the layer thicknesses observed with AFM (the same samples investigated by AFM were used). In acetonitrile, average thicknesses were found to be 16 ± 1 nm following one cyclic voltammetric scan and 32 ± 2 nm for three cycles, using an extinction coefficient k = 0.031 and refractive index n = 1.247 for polyaniline as an optical model[54]. These results are in good agreement with the values obtained by AFM, and tend to confirm the mechanism of polymerization at the surface as shown in Scheme 4.4 (Table 4.1).

Number of growth cycles	Ψ	Δ	Layer thickness Ellipsometry (nm)	Layer thickness AFM (nm)
1	32.22	168.95	16 ±1	15 ± 2
3	32.30	159.01	32 ±2	35 ± 2

Table 4.1 Layer thickness measurements by ellipsometry and AFM, in acetonitrile (Ψ and Δ are the ellipsometric angles calculated from the angles of the polarizer and the analyzer at the null point (point of lowest intensity)

4.5 X-ray photoelectron spectroscopy (XPS)

X-ray photoelectron spectroscopy was used to ascertain the nature of the functional groups present at the surface of the electrochemically formed layers. Figures 4.8 and 4.9 correspond to the overall XPS scans of etched (following the NH_4F treatment) and functionalized (following the nitro to amino group reduction step) Si substrates in acetonitrile, respectively.

The data obtained in the XPS scan for the etched substrate (Figure 4.8) indicates that the binding energy value of the Si 2p 3/2 is in the range of 99 to 100 eV, reported for Si(100) surfaces (compared to peak values in the range of 103 to 104 eV, reported for Si(100) O_2 species) [55] . It can be inferred that the chemical etching process is efficient at removing surface oxides, with a relatively small amount present after etching (O 1s at 531.7 eV). Weak N 1s and C 1s peaks are also visible which may be attributed to possible residue from the etching procedure (NH_4F treatment). After the electrochemical attachment of the aryl-nitro moiety and subsequent reduction of the nitro to amino groups (Figure 4.9), the XPS scan of a functionalized Si substrate indicates that atomic percentage of carbon(C 1s) and the nitrogen (N 1s) increased substantially, accompanied by the net appearance of the double peaks in the 405 eV region. The Si 2p peak is suppressed after functionalization and the C 1s peak appears at 285.1 eV, very close to the values for C-N bonds (it should be noted that the C 1s peak associated to benzene is also reported to appear in this region at approximately 284.7 eV)[55]. Figure 4.10 shows a high resolution view of the N 1s peaks appearing in Figure 4.9, which are readily attributable to those generated by nitrogen in phenyl-NH_2 and phenyl-NO_2 species, at approximately 401 and 406 eV, respectively[55]. It should be reiterated however that the

presence of electrochemically formed phenyl-NHOH, which is also expected to give a peak in the vicinity of 400 eV, can not be excluded. These results nevertheless tend to indicate that both nitro and amino functional groups are present following the final electrochemical reduction process (with NH_2 functional groups more likely near the surface and NO_2 groups more likely present in the bulk of the thick layers produced during the initial reduction step). The results presented in the following section on fluorescence measurements also tend to confirm that the functionalized surfaces thus produced are appropriate for further modification with glutaraldehyde, and subsequent oligonucleotide probe immobilization.

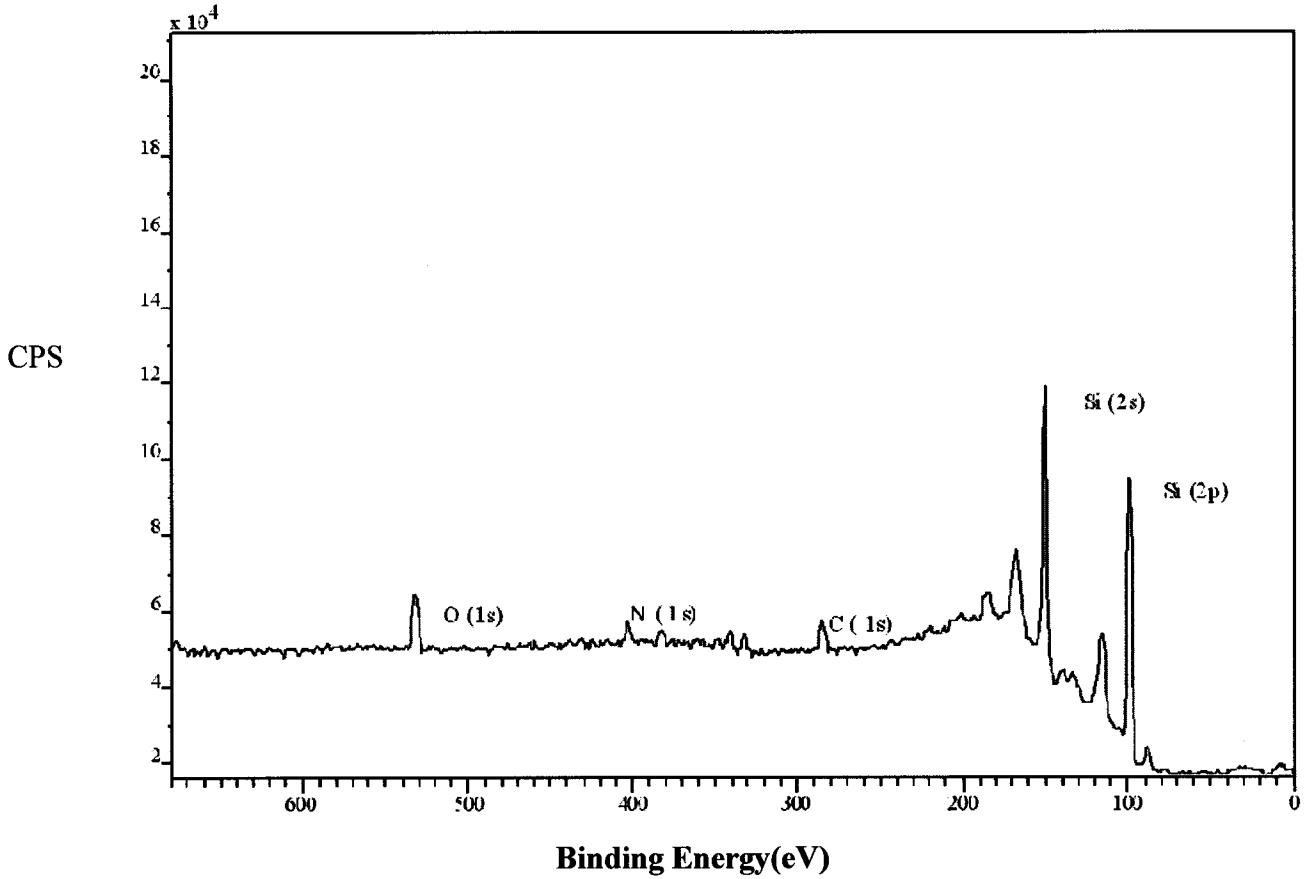

Figure 4.8 XPS of etched Si (100)

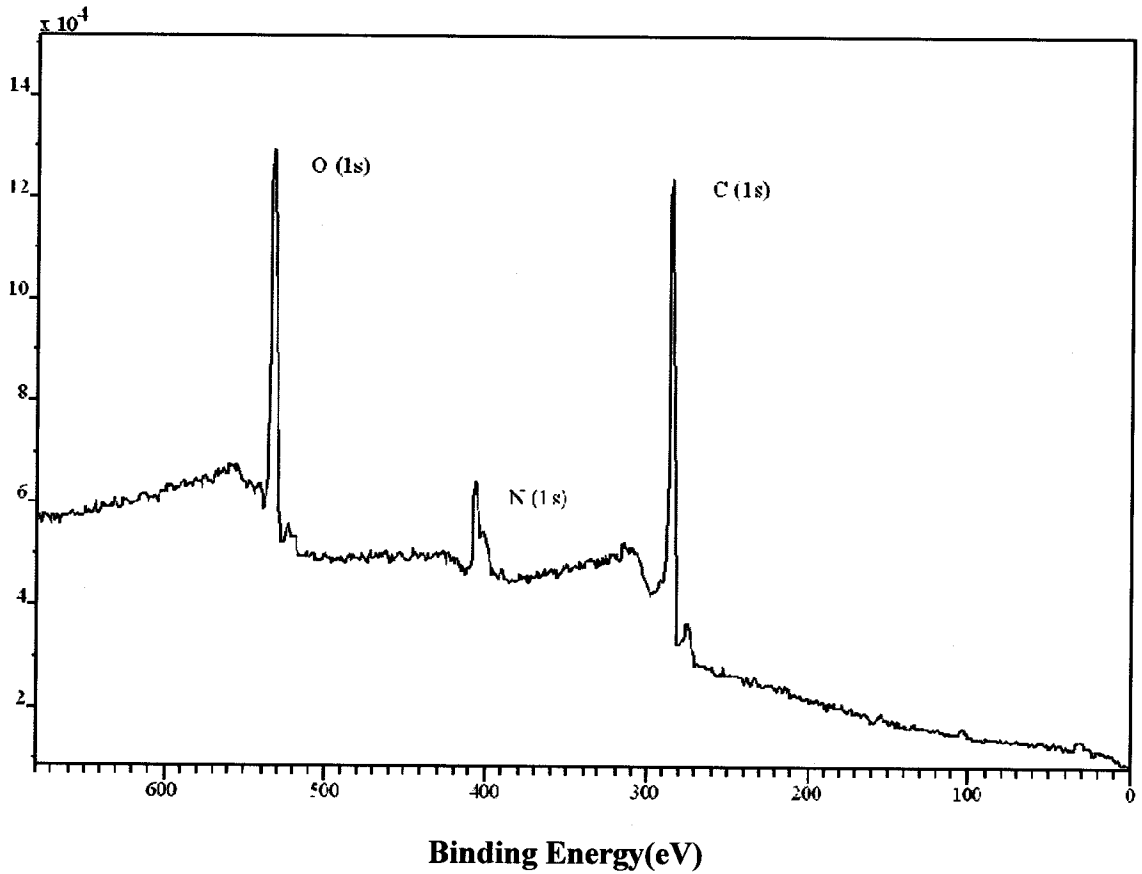

Figure 4.9 XPS of the silicon substrate following functionalization with 4-nitrobenzene and reduction of the nitro groups to amino groups

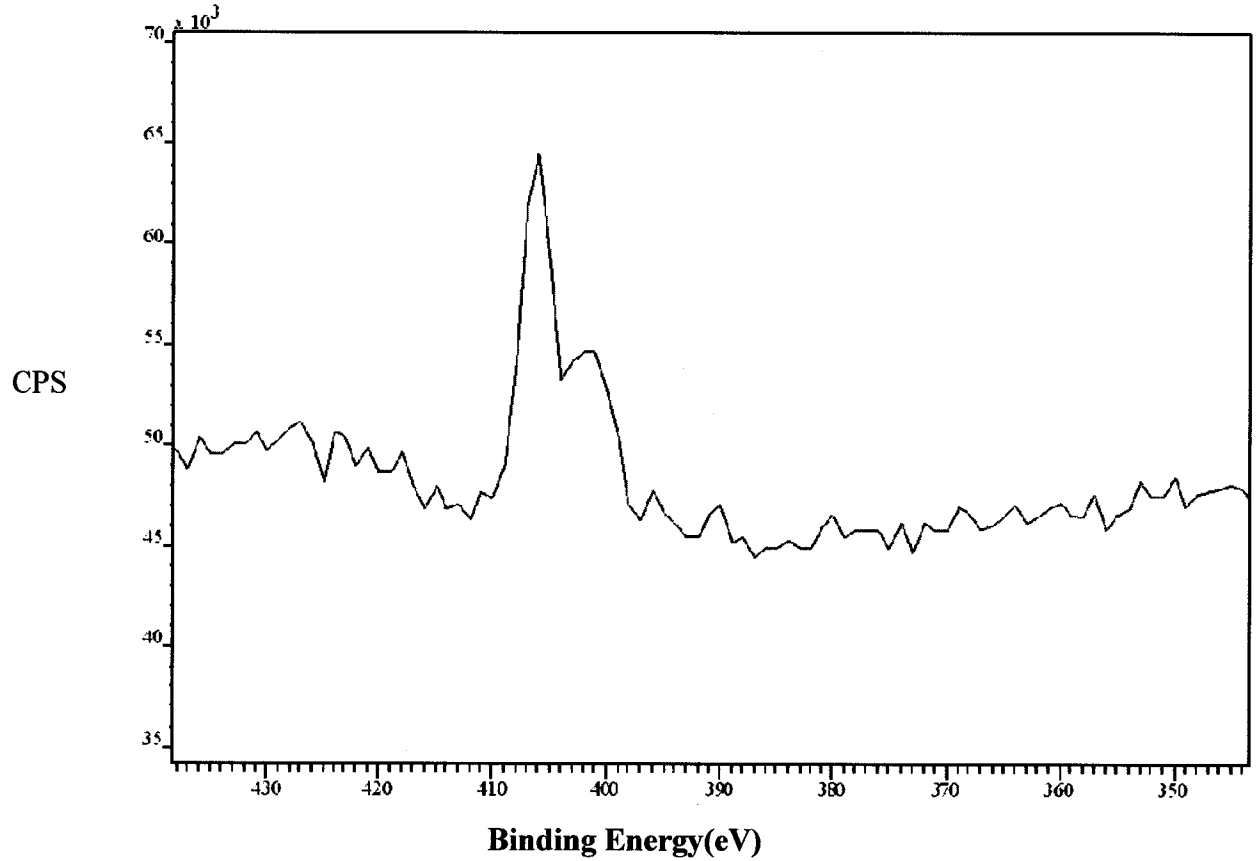

Figure 4.10 Nitrogen 1s peak for the functionalized silicon surface

4.6 Fluorescence Imaging

In light of the lower quality layers electrochemically generated in aqueous media (as revealed by the AFM images), only Si substrates initially functionalized in acetonitrile were employed to examine the probe/target hybridization event with fluorescence imaging. To test and confirm good reactivity of the aldehyde-amino linkage, preliminary experiments were performed using fluorescein-labelled (NH_2C_6)-$dT_{(20)}$ as probe sequences immobilized on surfaces with and without glutaraldehyde treatment (Figures 4.11A and B, respectively). The results clearly indicate that the probe sequences are bound to the surface (following extensive washing with the immobilization buffer and then with distilled-deionized water), with uniform coverage over the area delimited by the 5 mm diameter aperture of the working electrode holder, and that no adsorbed material remains after the washing procedure.

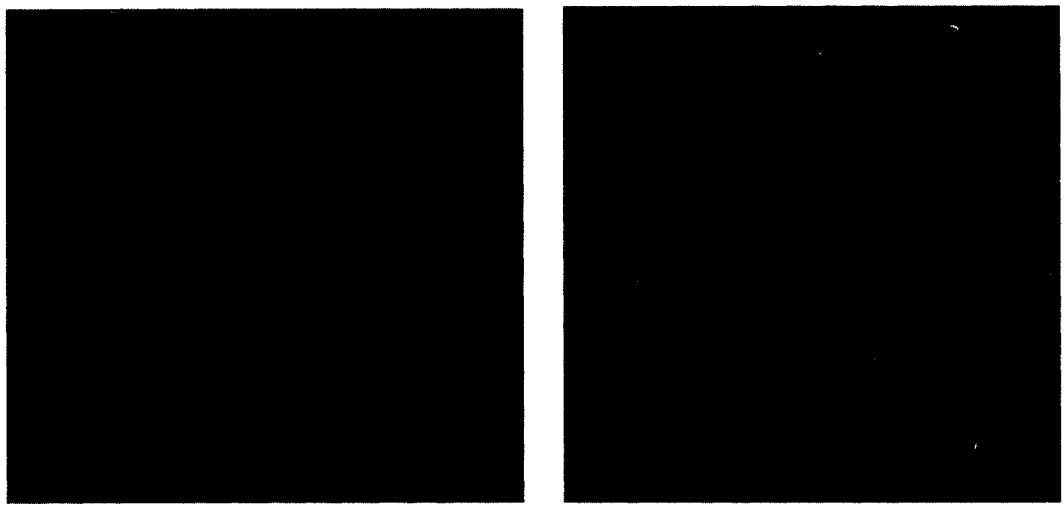

A B

Figure 4.11 Immobilization of fluorescein-labeled oligo $dT_{(20)}$ to the functionalized surface with glutaraldehyde treatment **(A)**, and without glutaraldehyde treatment **(B)**

Probe/target hybridization was then tested by placing Si chips with immobilized non-labelled $dT_{(20)}$ in contact with fluorescein-labelled $dA_{(20)}$ complementary target sequences (Scheme 4.5). The presence of the complementary sequences (following extensive washing with the hybridization buffer and then with distilled-deionized water) is clearly shown in Figure 4.12B. No hybridization was observed with the fluorescein-labelled $dA_{(20)}$ target, when a non-complementary random sequence ((NH_2C_6)-(AGTCCATTGCAGTCCATTGC)) was used as the immobilized probe (Figure 4.12B).

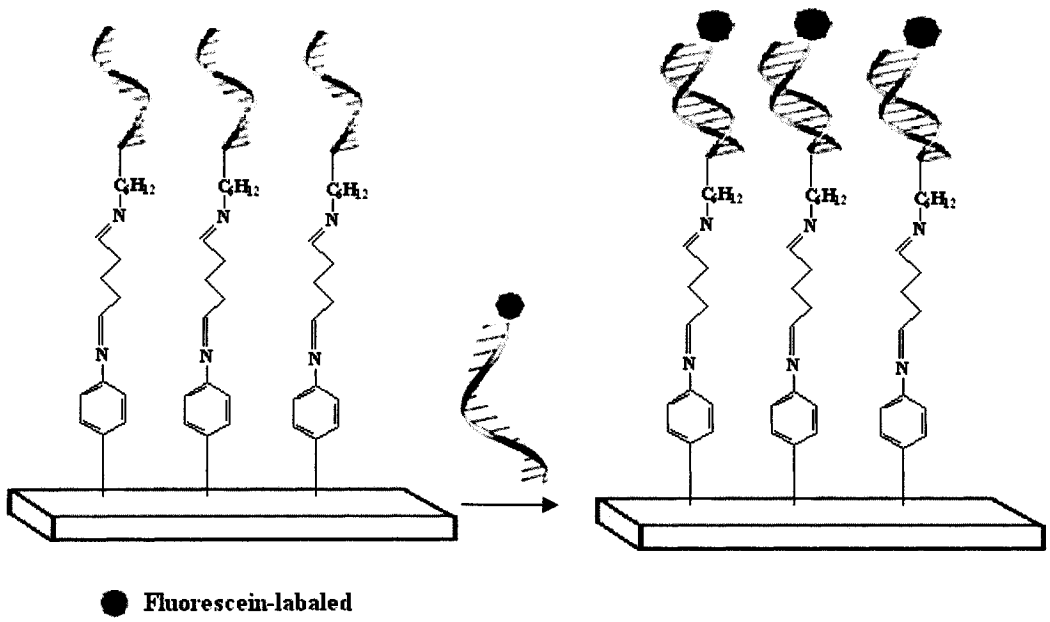

Scheme 4.5: Hybridization of immobilized oligonucleotides

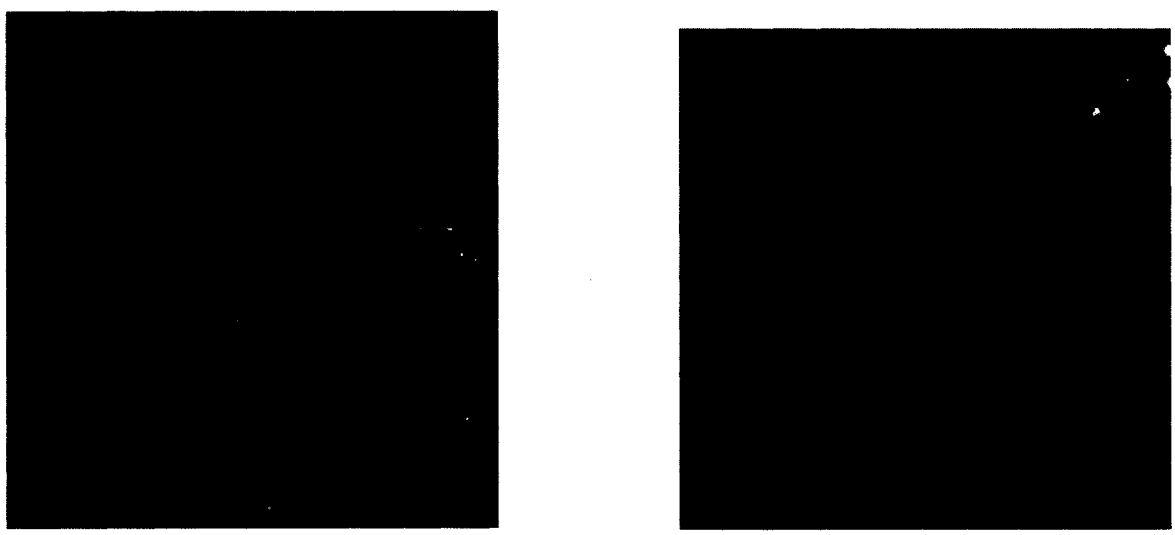

A B

Figure 4.12 Hybridization of fluorescein-labeled oligo $dA_{(20)}$ target to the complementary oligo $dT_{(20)}$ probe layer **(A)**. Hybridization of the fluorescein-labeled oligo $dA_{(20)}$ target to the non-complementary random sequence probe layer **(B)**

These results provide a solid indication of the feasibility of the diazonium-based, electrochemical functionalization approach for the fabrication of silicon-based DNA sensors.

4.7 Screen-printed carbon electrodes (SPEs)

Practical electrochemical biosensors require simple and inexpensive fabrication techniques. Screen-printed carbon electrodes (SPEs), also considered as interesting candidates for this purpose, have been shown to be an attractive substrate for immobilization of biomolecules because of their versatility and their potential for producing disposable, low-cost devices. Early SPEs were initially used to detect glucose in blood samples, but now they are being used to detect other biomolecules, metals, and anions[56].

In line with the work on functionalization of Si chips previously described, the electrochemical functionalization of screen-printed carbon elelctrodes for DNA immobilization was also explored. The SPE platform for this purpose was designed to provide multi-probe capability, easily produced by screen-printing of the polyester carbon ink using a Dek 248 screen-printing machine, as described in the experimental section. Each SPE network is composed of one ring-shaped reference electrode and one central auxiliary electrode, surrounded by eight 780 μm^2 working electrodes (Figure 4.13). Each of the working electrodes can be individually addressed, and therefore functionalized, through the individual contacts. The advantage of this approach is the ease of fabrication, the low cost (disposability), and the fact that the pattern can be easily adapted to specific needs (changing the configuration and the number of working electrodes only requires producing the mask). In addition, with the particular network shown in Figure 4.13 for example, one can carry out electrochemistry on one drop (30 μL) of solution.

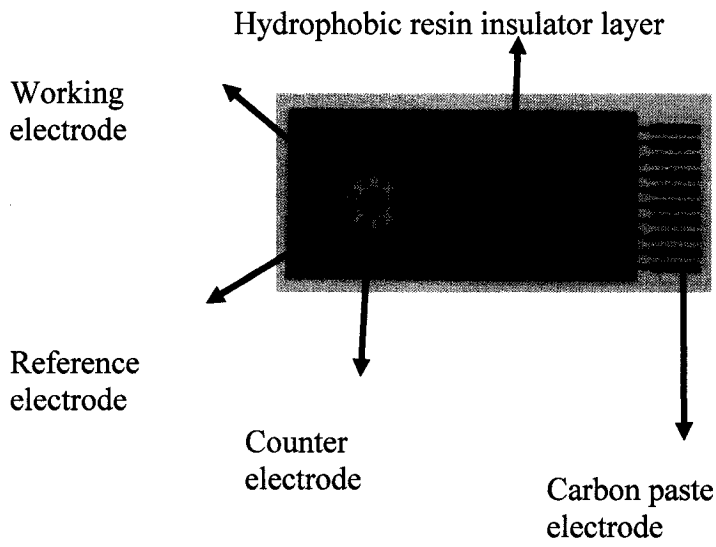

Figure 4.13 Features of a screen-printed-electrode

4.7.1 Functionalization of SPEs with EDC using chronoamperometry

1-Ethyl-3-(3-dimethylaminopropyl)-carbodiimide (EDC) is a water soluble carbodiimide derivative well known to facilitate the formation of amide bonds between carboxylic acids and amines[57]. EDC can be used as an immobilization reagent in the preparation of affinity gels[57]. The immobilization of ligands using EDC can be carried out in two ways: (*i*) a carboxyl group can be used to couple with an amine-containing ligand or (*ii*) in the reverse manner, where an amine-containing support is coupled with a carboxyl-containing ligand. In most reactions, a spacer molecule containing the required terminal group is first coupled to the surface and then EDC is used to immobilize the ligand. The ideal pH for this reaction is 4.75 but the reaction can be carried out in a pH range of 4.5-7.5 as well (Scheme 4.6) [57].

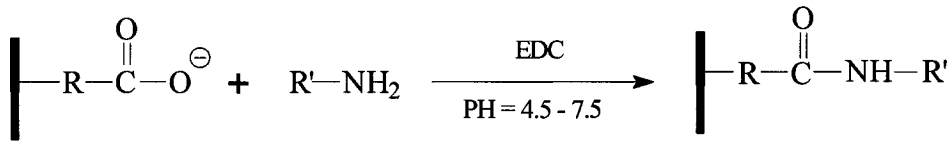

Scheme 4.6 Immobilization of an amine-containing ligand through a carboxylate terminated spacer (R = carbon chain)

The electrochemical approach to functionalize the SPEs used in this work consists of performing chronoamperometry in the presence of EDC, by applying a potential of +2.2 V (using the carbon ring as a pseudo reference, Fig. 4.13) to oxidize the carbon and generate carboxyl groups on the surface (Figure 4.14) [58].

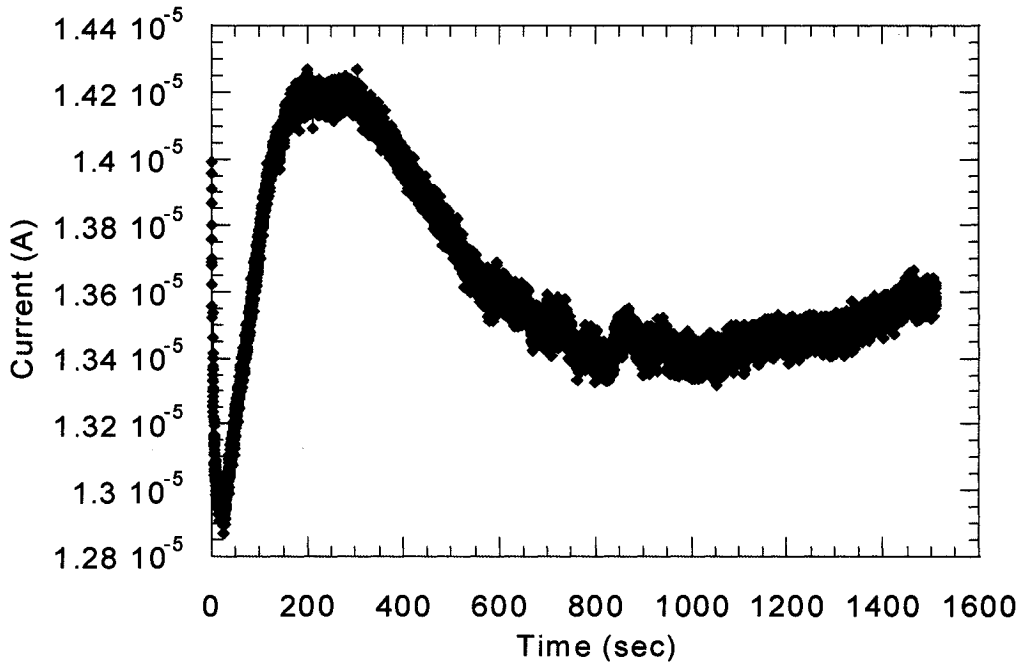

Figure 4.14 Chronoamperometry of SPE in the presence of EDC

The carboxyl groups then react with the EDC and produce an ester intermediate that can react with the amino group of the oligonucleotides, resulting in the covalent attachment of the oligonucleotide to the surface (Scheme 4.7) [57].

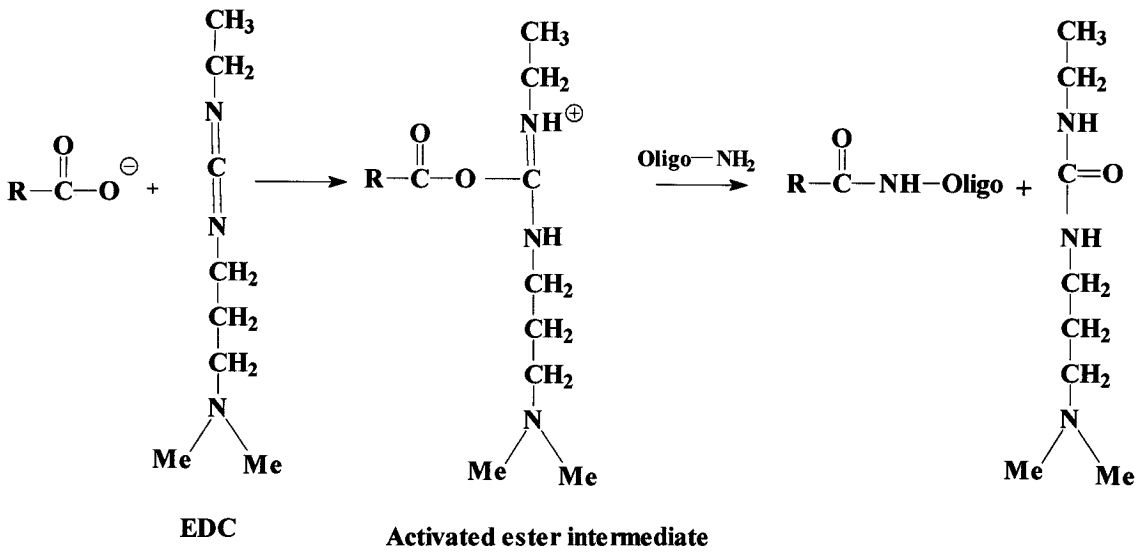

Scheme 4.7 Reaction of EDC at the activated carbon surface, and covalent binding to the amino linker of the oligonucleotide

The attachment of oligonucleotides to the SPE surface was then investigated using AFM as well as fluorescence imaging.

4.7.2 AFM Images of immobilized oligo dT (20-mer and 200-mer)

Figure 4.15B shows an AFM image of an SPE modified with oligo dT 20-mer, following functionalization with EDC (Figure 4.15A).

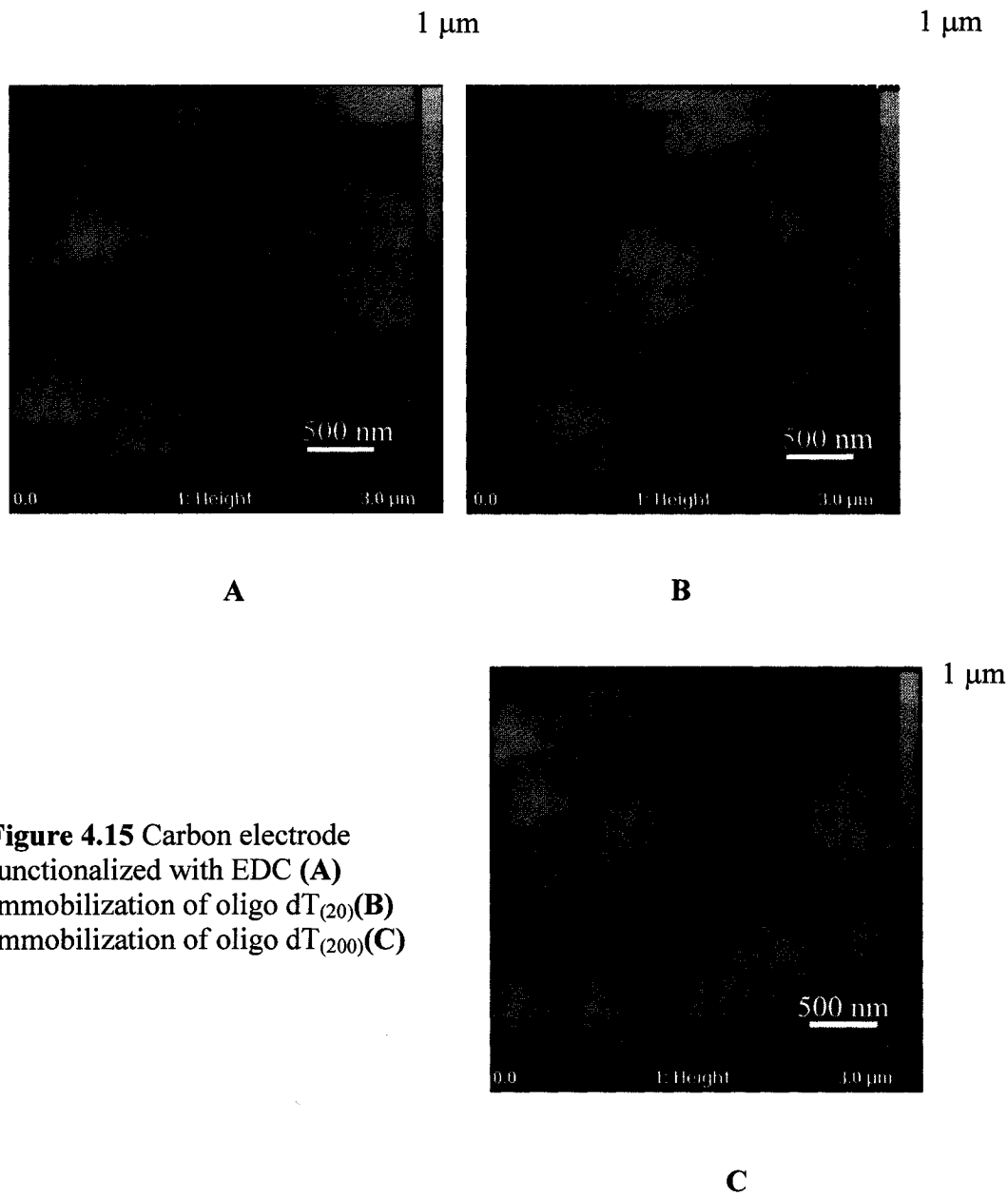

Figure 4.15 Carbon electrode functionalized with EDC **(A)** Immobilization of oligo $dT_{(20)}$**(B)** Immobilization of oligo $dT_{(200)}$**(C)**

The two images (4.15 A and B) show little change in the surface features following immobilization of the oligo dT 20-mer. However, when a sequence of ten times longer length (oligo dT 200-mer) is immobilized onto the EDC functionalized surface, a fine structure can be distinguished which is believed to be due to the presence of the DNA sequences (Figure 4.15C). The immobilization of DNA to the carbon network was confirmed by fluorescence microscopy.

4.7.3 Fluorescence imaging of immobilized ssDNA onto SPEs

Fluorescein-labeled (NH_2C_6)-oligod$T_{(20)}$ was covalently attached at the electrochemically functionalized carbon surface and fluorescence imaging was performed (Figure 4.16).

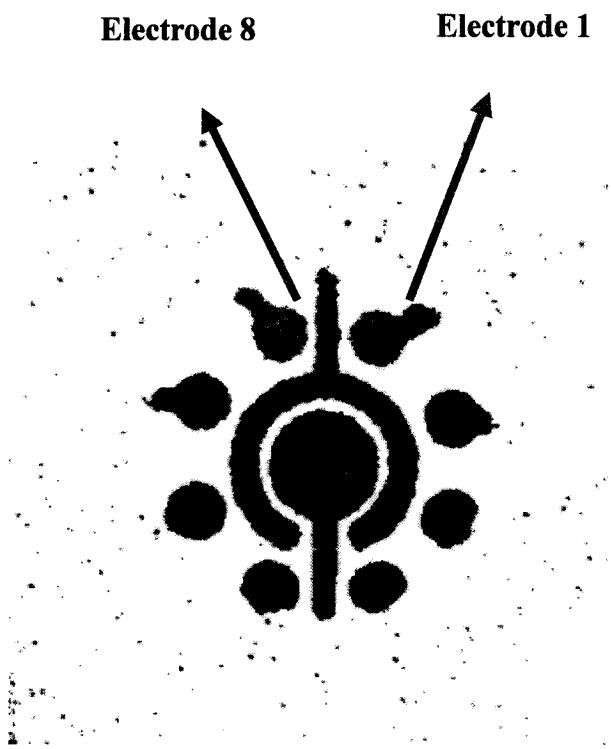

Figure 4.16 Fluorescence image of SPE network with immobilized ssDNA

The eight working electrodes of the SPE network can be individually addressed for electrochemical functionalization. As shown in Figure 4.16, immobilization of the fluorescein labeled ssDNA occurs at electrodes 1 and 8 on the SPE, which were the only electrodes previously functionalized with EDC. A control experiment was performed in the absence of carbodiimide (no electrochemical functionalization of the SPE), and in this case no fluoresence signal was observed following the immobilization procedure of the labeled sequence, indicating that EDC is required for amide bond formation. This measurement is important for illustrating successful immobilization and the absence of non-specific binding at the surface of the SPE network.

4.8 Direct DNA detection by electrochemical impedance measurements

4.8.1 Impedance measurement after attachment of glutaraldehyde

In this final section, Si chips were used to demonstrate the ability of the electrochemically functionalized sensors to directly detect DNA sequences in liquid media. As described in the theory part, impedance (Z_i) measurements can provide direct information on the variation of capacitance in the EIS structure due to semiconductor surface modification. These variations in capacitance are readily monitored through changes in the flat-band potential of the semiconductor (V_{fb}), which is determined by extrapolating the slope of the Z_i curve in the depletion region to the x-axis (dc potential).

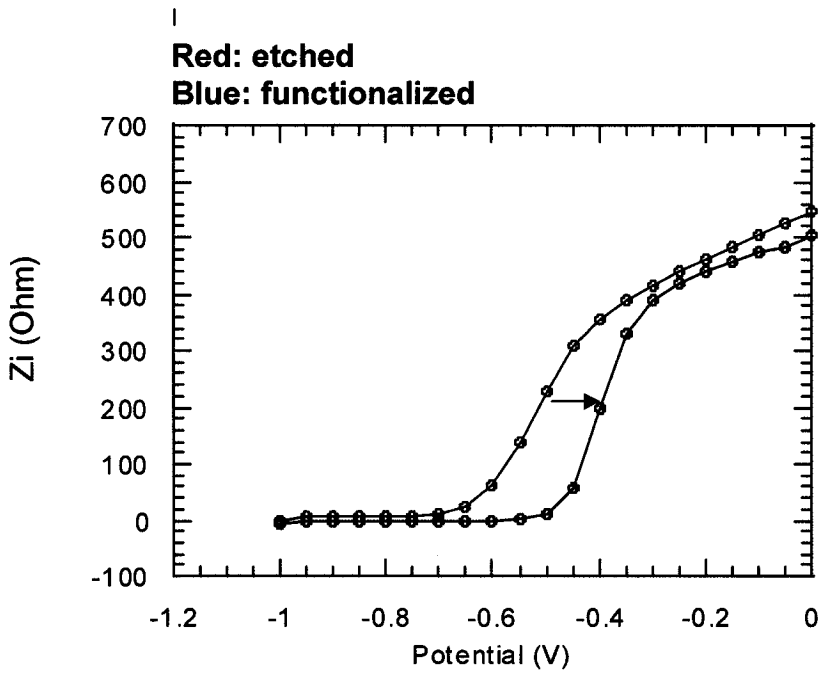

Figure 4.17 Shift of the imaginary impedance following the full functionalization (electrochemical and glutaraldehyde treatment) of a Si substrate

These measurements are exemplified in Figure 4.17, which shows a shift in the Z_i curve caused by the overall functionalization steps (electrochemical nitro diazonium reduction, reduction of nitro to amino groups, and the glutaraldehyde treatment). A positive shift in V_{fb} of approximately 200 mV (corresponding to a 250 ohms decrease in Z_i at a fixed dc potential of -0.4 V in the depletion region) is observed in going from the etched to the glutaraldehyde treated Si surface.

4.8.2 Impedance detection of oligonucleotide hybridization

Figures 4.18 and 4.19 illustrate the shifts observed due to the hybridization event between immobilized (NH_2C_6)-oligo$(dT)_{20}$ and the complimentary oligo$(dA)_{20}$ homooligonucleotide sequences, and between immobilized (NH_2C_6)-ACT-CCA-TTG-CAG-TCC-ATT-GC and the complementary TGA-GGT-AAC-GAC-AGG-TAA-CG random sequences, respectively.

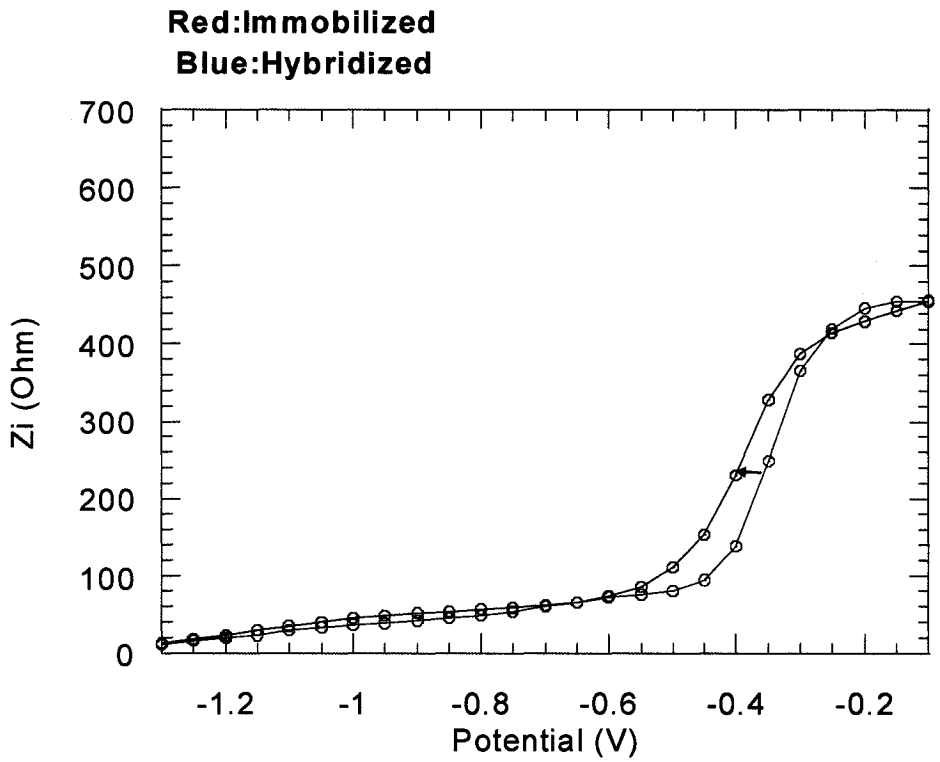

Figure 4.18 Imaginary impedance as a function of the dc potential for the immobilized oligo$(dT)_{20}$ (red circles) and hybridized oligo$(dA)_{20}$ after 120 min of hybridization time (blue circles)

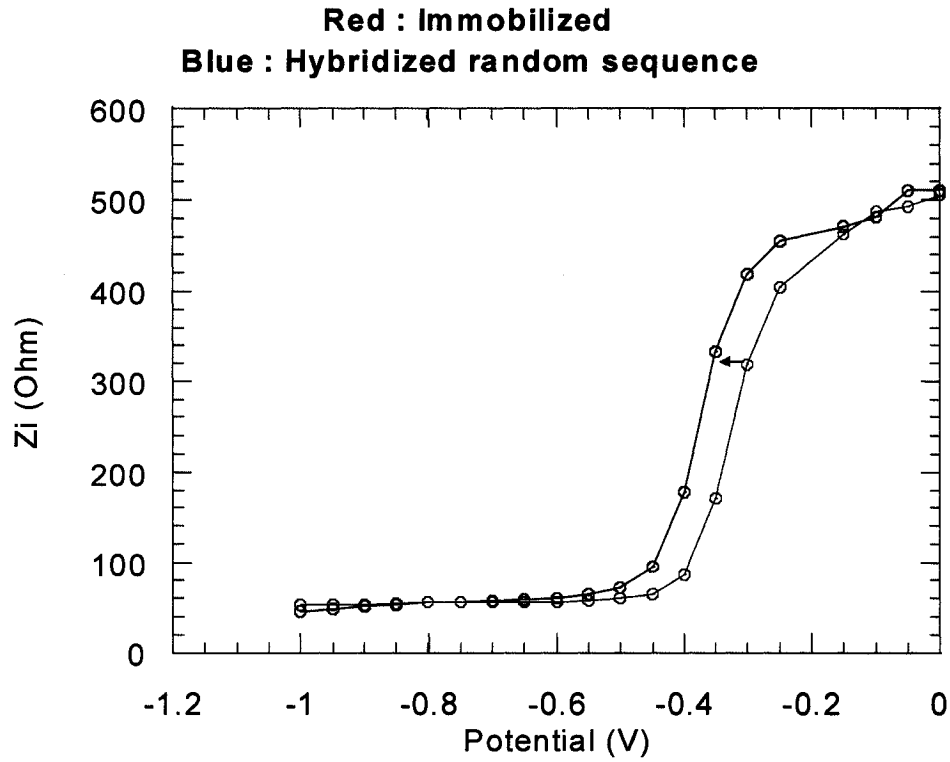

Figure 4.19 Imaginary impedance as a function of the dc potential for the immobilized (red circles) and hybridized random sequence after 120 min of hybridization time (blue circles).

In the case of the homooligonucleotide sequences, a negative shift in flat-band potential of -50 mV was observed for the hybridization event, corresponding to a 90 Ohms increase in Z_i at a fixed dc potential of -0.4 V in the depletion region (Figure 4.18). In the case of random sequences a similar signal is observed, with a negative shift in flat-band potential of -75 mV for the hybridization event, corresponding to a 160 Ohms increase in Z_i at a fixed dc potential of -0.35 V in the depletion region (Figure 4.19).

The impedance shift due to the hybridization of the random sequence is larger than the shift obtained for the hybridization of the homooligonucleotide sequence. These variations in response may indicate how perfectly the complementary strand can hybridize with the probe layer, for the random sequence, as opposed to the homooligonucleotide sequence where there are many possibilities for incomplete hybridization.

As a control experiment a blank sample (everything except the target random DNA sequence) was run to determine if shifts would be observed in the impedance measurements. As shown in Figure 4.20 no shift was observed due to the buffer or electrolyte solutions.

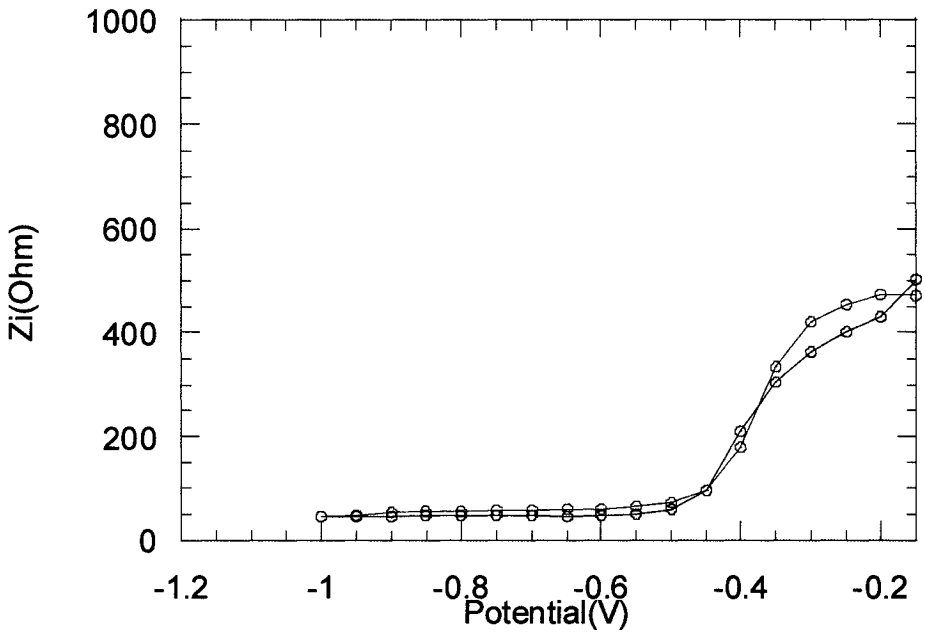

Figure 4.20 Imaginary impedance as a function of the dc potential for the blank sample (immobilized random probe sequence in the absence of the complementary target sequence) before (red circles) and after (blue circles) the hybridization step

5.1 Conclusions

In this work, two different methods were used to modify surfaces for covalent attachment of single stranded DNA probe sequences. In the first protocol, short oligonucleotides covalently attached to a modified silicon surface, through a glutaraldehyde linker, were found to hybridize with their complementary strands. Before immobilization of the oligonucleotide, the surface was functionalized *via* the simple and rapid electrochemical reduction of a diazonium salt in aqueous and acetonitrile media. The films were characterized using AFM and ellipsometry and the results indicate that more uniform and homogeneous films formed in acetonitrile rather than aqueous media, possibly due to the reduction of water causing evolution of hydrogen bubbles at the electrode surface. Furthermore, layer thicknesses were measured after producing holes in the organic films. In acetonitrile, the single voltammetric scan thickness was found to be approximately 15 nm, whereas for three scans the layer thickness was found to be approximately 35 nm. Ellipsometry measurements of layer thicknesses were in agreement with the AFM results. XPS analysis reveals that, although the electrochemical functionalization approach was successful, the modified silicon surfaces are characterized by the presence of both nitro and amino groups (with the possibility also of NHOH groups in small amounts). Fluorescence images were taken which confirm the immobilization of ssDNA and hybridization of complementary strands with probe oligonucleotide sequences attached to the surface. No hybridization was observed using a non-complementary random sequence.

In the second protocol, screen-printed carbon electrodes (individually addressable within a multi-electrode network) were electrochemically functionalized using 1-ethyl-3-(3-dimethylaminopropyl)-carbodiimide (EDC), under an applied potential of +2.2 V in aqueous acidic media. Single stranded (NH_2C_6)-oligonucleotide probe sequences were attached to these functionalized carbon surfaces, and their presence was probed with AFM. The AFM image following the attachment of a 20mer sequence shows little difference with that of an EDC modified electrode. However, evidence of the presence of attached DNA does seem to appear when a 200mer is attached as the probe layer. The attachment of 20mers was nevertheless confirmed by conventional fluorescence measurements. Direct detection of DNA sequences was tested using these silicon based sensors. Electrochemical impedance measurements performed on random and homooligonucleotide DNA sequences clearly show shifts in the imaginary impedance due to hybridization. This work demonstrates the feasibility of simple electrochemical approaches to functionalize surfaces for the immobilization of biomolecules, and their important potential for future biosensor development.

5.2 Future Work

Additional improvements in device efficiency could be achieved by addressing the following aspects:

1) Reduce the thickness of the electrochemically generated layers on the silicon surfaces.

The closer the probe layer is to the surface of the semiconductor the greater the effect of the hybridization event on the electrical signal (shift of flat-band potential). Important factors that influence the thickness and structure of films formed by electrochemical reduction of the aryl diazonium include: scan rate, the number of cyclic voltammetric scans, the applied potential, the particular substrate, and the concentration of the aryl diazonium. These parameters can potentially be adjusted (low concentration of aryl diazonium, short electrolysis time/faster san rate) to reduce layer thicknesses and ideally achieve monolayer formation.

2) Correlate the probe density to optimize hybridization efficiency and therefore the sensitivity of the sensors.

3) Test the ability of the direct impedance approach to discriminate between perfectly matched sequences and those with a single base mismatch. This is important for potential clinical applications.

4) Perform single molecule force measurements between two DNA strands through surface modification of the chips and the AFM tips themselves [59-61]. Since

electrochemical modification of the AFM tips through the reduction of the diazonium salt would be technically difficult, other protocols such as chemical silanization could be employed.

References

(1) Souteyrand, E.; Cloarec, J. P.; Martin, J. R.; Wilson, C.; Lawrence, I.; Mikkelsen, S.; Lawrence, M. F. *Journal of Physical Chemistry B* **1997**, *101*, 2980-2985.

(2) Cloarec, J. P.; Deligianis, N.; Martin, J. R.; Lawrence, I.; Souteyrand, E.; Polychronakos, C.; Lawrence, M. F. *Biosensors & Bioelectronics* **2002**, *17*, 405-412.

(3) Martin, J. R.; Souteyrand, E.; Lawrence, M. F.; Mikkelsen, S. R. *US Patent 6* **2000**, 150.

(4) Ramsay, G. *Nature biotechnology* **1998**, *16*, 40-44.

(5) Sam, M.; Boon, E. M.; Barton, J. K.; Hill, M. G.; Spain, E. M. *Langmuir* **2001**, *17*, 5727-5730.

(6) Zhou, D.; Sinniah, K.; Abell, C.; Rayment, T. *Langmuir* **2002**, *18*, 8278-8281.

(7) Ruffien, A.; Dequaire, M.; Brossier, P. *Chemical Communications (Cambridge, United Kingdom)* **2003**, 912-913.

(8) Azek, F.; Grossiord, C.; Joannes, M.; Limoges, B.; Brossier, P. *Analytical Biochemistry* **2000**, *284*, 107-113.

(9) Hu, J.; Wang, M.; Weier, H. U. G.; Frantz, P.; Kolbe, W.; Ogletree, D. F.; Salmeron, M. *Langmuir* **1996**, *12*, 1697-1700.

(10) Marquette, C. A.; Lawrence, I.; Polychronakos, C.; Lawrence, M. F. *Talanta* **2002**, *56*, 763-768.

(11) Macanovic, A.; Marquette, C.; Polychronakos, C.; Lawrence, M. F. *Nucleic Acids Research* **2004**, *32*, e20/21-e20/27.

(12) Lamture, J. B.; Beattie, K. L.; Burke, B. E.; Eggers, M. D.; Ehrlich, D. J.; Fowler, R.; Hollis, M. A.; Kosicki, B. B.; Reich, R. K.; Smith, S. R. *Nucleic Acids Res* **1994**, *22*, 2121 - 2125.

(13) Lenigk, R.; Carles, M.; Ip, N. Y.; Sucher, N. J. *Langmuir* **2001**, *17*, 2497-2501.

(14) Delamar, M.; Hitmi, R.; Pinson, J.; Saveant, J. M. *J. Am. Chem. Soc* **1992**, *114*, 5883-5884.

(15) de Villeneuve, C. H.; Pinson, J.; Bernard, M. C.; Allongue, P. *Journal of Physical Chemistry B* **1997**, *101*, 2415-2420.

(16) Brooksby, P. A.; Downard, A. J. *Journal of Physical Chemistry B* **2005**, *109*, 8791-8798.

(17) D'Amours, M.; Belanger, D. *J. Phys. Chem. B* **2003**, *107*, 4811-4817.

(18) Matrab, T.; Chehimi, M. M.; Perruchot, C.; Adenier, A.; Guillez, A.; Save, M.; Charleux, B.; Cabet-Deliry, E.; Pinson, J. *Langmuir* **2005**, *21*, 4686-4694.

(19) Kariuki, J. K.; McDermott, M. T. *Langmuir* **1999**, *15*, 6534-6540.

(20) Kariuki, J. K.; Mc Dermott, M. T. *Langmuir* **2001**, *17*, 5947-5951.

(21) Downard, A. J.; Roddick, A. D.; Bond, A. M. *Analytica Chimica Acta* **1995**, *317*, 303-310.

(22) Dequaire, M.; Degrand, C.; Limoges, B. *J. Am. Chem. Soc* **1999**, *121*, 6946-6947.
(23) Brooksby, P. A.; Downard, A. J. *Langmuir* **2004**, *20*, 5038-5045.
(24) Ghilane, J.; Delamar, M.; Guilloux-Viry, M.; Lagrost, C.; Mangeney, C.; Hapiot, P. *Langmuir* **2005**, *21*, 6422-6429.
(25) Wang, J.; Firestone, M. A.; Auciello, O.; Carlisle, J. A. *Langmuir* **2004**, *20*, 11450-11456.
(26) Allongue, P.; Villeneuve, C. H.; Pinson, J. *Electrochimica Acta* **2000**, *45*, 3241-3248.
(27) Wang, J. *Nucleic Acids Research* **2000**, *28*, 3011-3016.
(28) Piunno, P. A. E.; Krull, U. J.; Hudson, R. H. E.; Damha, M. J.; Cohen, H. *Analytical Chemistry* **1995**, *67*, 2635-2643.
(29) Hang, T. C.; Guiseppi-Elie, A. *Biosensors & Bioelectronics* **2004**, *19*, 1537-1548.
(30) Willner, I.; Patolsky, F.; Weizmann, Y.; Willner, B. *Talanta* **2002**, *56*, 847-856.
(31) Cha, J.; Han Jung, I.; Choi, Y.; Yoon Dae, S.; Oh Kwang, W.; Lim, G. *Biosensors & bioelectronics* **2003**, *18*, 1241-1247.
(32) Millan, K. M.; Saraullo, A.; Mikkelsen, S. R. *Analytical chemistry* **1994**, *66*, 2943-2948.
(33) Moran, L. A.; Scrimgeour, K. G.; Horton, H. R.; Ochs, R. S.; Rawn, J. D. *Biochemistry*; Prentice-Hall Inc: New Jersey, 1994.
(34) Watson, J. D.; Crick, F. H. *Nature* **1953**, *171*, 737-738.
(35) Mainwaring, W. I. P.; Parish, J. H.; Pickering, J. D.; Mann, N. H. *Nucleic Acid Biochemistry and Molecular Biology*; Blackwell Scientific Publications: Oxford, 1982.
(36) Adams, L. P.; Knowler, T.; Laeder, D. P. *Biochemistry of Nucleic Acids*; Chapman & Hall: London, New York, 1992.
(37) Brett, C. M. A.; Brett, A. M. O. *Electrochemistry:Principles, Methods and Application*; Oxford university press Inc: Oxford, New York, 1993.
(38) Bard, A. J. *Electroanalytical Chemistry*: New York and Basel, 1966.
(39) Bard, A. J.; Faulkner, L. R. *Electrochemical Methods:fundamentals and applications*; Wiley: New York, 2001.
(40) Finklea, H. O. *Semiconductor Electrodes*; Amesterdam, New York, Elsevier: Netherlands, 1988.
(41) Binnig, G.; Rohrer, H. *Surface Science* **1983**, *126*, 236-244.
(42) Binnig, G.; Rohrer, H. *Ultramicroscopy* **1983**, *11*, 157-160.
(43) Miles, M. *Science (Washington, D. C.)* **1997**, *277*, 1845, 1847.
(44) Binnig, G.; Rohrer, H. *Helvetica Physica Acta* **1982**, *55*, 726-735.
(45) Binning, G.; Quate, C. F.; Gerber, C. *Phys.Rev.Lett* **1986**, *56*, 930-933.
(46) Morris, V. J.; Kirby, A. R.; Gunning, A. P. *Atomic force microscopy for biologist*; London : Imperial College Press ; Singapore ; River Edge, NJ : Distributed by World Scientific Pub, 1999.
(47) Binnig, G.; Smith, D. P. E. *Review of Scientific Instruments* **1986**, *57*, 1688-1689.
(48) Fahlman, A.; Siegbahn, K. *Arkiv foer Fysik* **1966**, *32*, 111-129.
(49) Riveiere, J. C.; Myhra, S. *Handbook of Surface and Interface Analysis*; Marcel Dekker Inc: New York, 1998.

(50) Nefedov, V. I. *X-ray photoelectron spectroscopy of solid surfaces*; VSP: Netherlands, 1988.
(51) Marquette, C. A.; Lawrence, M. F.; Blum, L. J. *Analytical Chemistry* **2006**, *78*, 959-964.
(52) Allongue, P.; Delamar, M.; Desbat, B.; Fagebaume, O.; Hitmi, R.; Pinson, J.; Saveant, J.-M. *J. Am. Chem. Soc.* **1997**, *119*, 201-207.
(53) Kariuki, J. K.; McDermott, M. T. *Langmuir* **2001**, *17*, 5947-5951.
(54) Abrantes, L. M.; Correia, J. P.; Savic, M.; Jin, G. *Electrochimica Acta* **2001**, *46*, 3181-3187.
(55) Moulder, J. F. *Handbook of X-ray Photoelectron Spectroscopy, 1st edition*; Elmer Corporation, Eden Prairie, Minnesota., 1992.
(56) Hart, J. P.; Wring, S. A. *Trends in analyticalchemistry* **1997**, *16*, 89-103.
(57) Hermanson, G. T.; Mallia, A. K.; Smith, P. K. *Immobilized affinity ligand techniques*; Academic Press: San Diego, 1992.
(58) Marquette, C. A.; Blum, L. J. *Sensors and Actuators B* **1998**, *51*, 100-106.
(59) Boland, T.; Ratner, B. D. *Proceedings of the National Academy of Sciences* **1995**, *92*, 5297-5301.
(60) Sattin, B. D.; Pelling, A. E.; Goh, M. C. *Nucleic Acids Research* **2004**, *32*, 4876-4883.
(61) Krautbauer, R.; Rief, M.; Gaub, H. E. *Nano Letters* **2003**, *3*, 493-496.

Appendix

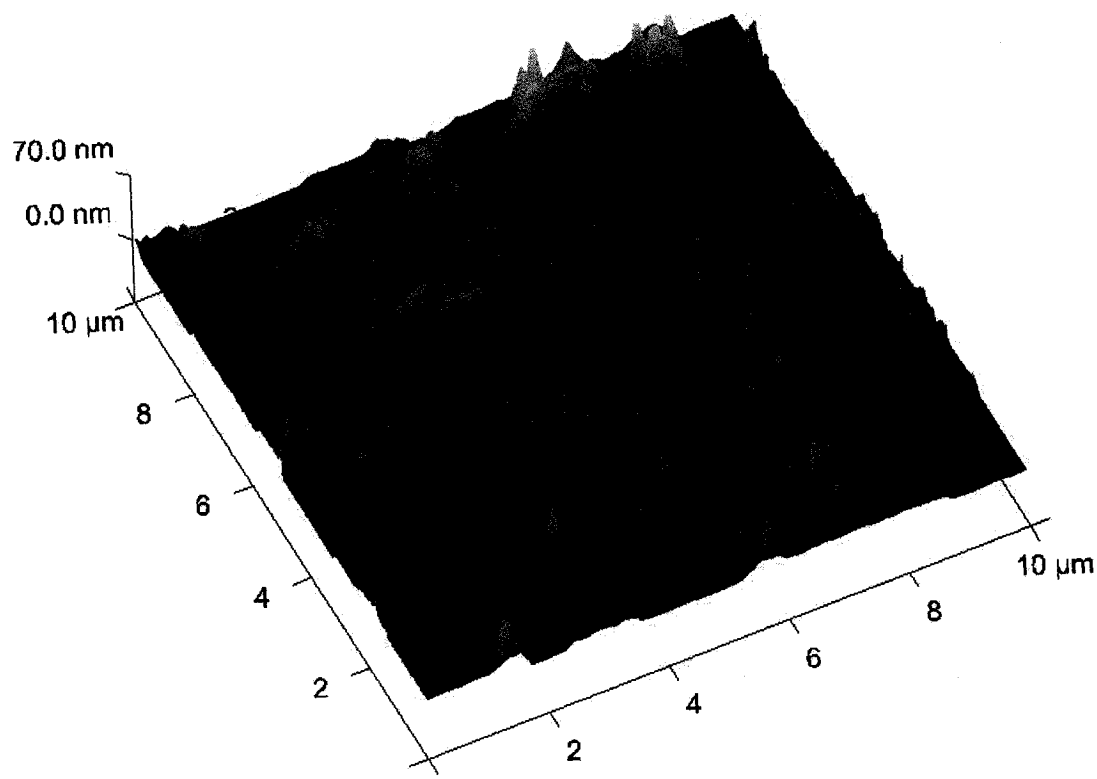

3D AFM image of Si functionalized with diazonium in aqueous media